

UNIVERSITY OF NAIROBI
DEPARTMENT OF GEOLOGY

MSc GEOLOGY (Applied Geophysics)

DELINEATION OF GOLD TARGET ZONES AND QUARTZ VEINS USING
INDUCED POLARIZATION AND RESISTIVITY MEASUREMENTS AT KAMWANGO
GOLD FIELD, MIGORI COUNTY, KENYA.

By
Joseph Njuguna Komu
B.Sc (Mining and Mineral Processing Engineering) J.K.U.AT, 2011.
Reg No: I56/70607/2013

A dissertation submitted to the Department of Geology as a requirement for the
award of the degree of Master of Science in Geology (Applied Geophysics) of the
University of Nairobi.

2016

DECLARATION

I declare that the work contained in this dissertation is my original work and has not been submitted for a degree at any other University. To the best of my knowledge, the dissertation contains no material previously published or written by other authors except where due reference is made.

Signature _____ Date: _____
Joseph Njuguna Komu.

I confirm that the candidate under my supervision has undertaken the work in this dissertation report.

Signature _____ Date: _____

Prof. Justus Barongo
Department of Geology, University of Nairobi.

ABSTRACT

A combined Induced Polarization and Resistivity survey was carried out in Kamwango area to delineate drill targets that would help plan an extended drill program. Gold potential in the area is evident by the extensive artisanal workings in the area. Given the high economic value of gold and its economic effect on the local community, there was need to initiate ways to efficiently define the mineralization.

IP and Resistivity methods, being some of the most effective geophysical methods for gold exploration, were used to map possible mineralization, employing advanced processing techniques to enhance interpretation, focusing the exploration program and minimizing risks before deciding to drill.

The research employed IP and Resistivity survey equipment to acquire: 1. Gradient data showing IP and Resistivity anomalous zones, 2. Pole-dipole data acquired over revealed gradient anomalies and tracing the anomalous zones to depth. The data were then processed using Oasis Montaj software and inverted using Res2dinv software to facilitate interpretation.

Six possible mineralized zones were identified from the study area, the zones are quite extensive, trend NW-SE and continuous as they extend from one survey line to the next. The NW-SE trend is consistent with the general trend of geological formations and structural formlines. The zones are most prominent in the Kamwango shear zone and the agglomerates with some zones occurring near the contact between the agglomerate and the Kamwango shear zone and another zone near the agglomerates and vesicular lava contact. The fact that one of the zones occurs in the area where previous boreholes were drilled by the license holder shows that the methods were a success and quite useful in the survey of this type of gold mineralization. A total of nine boreholes were proposed for follow-up drilling from the interpreted results.

ACKNOWLEDGEMENT

I would like to sincerely thank everyone who has helped me in my journey to completion of this thesis. First and foremost, thanks to the Almighty God through whom everything is possible.

Thanks to the University of Nairobi, Department of Geology for their instruction and guidance. Special thanks to my supervisor Prof J.Barongo for always making time for me, your comments and criticism, advise, support and encouragement through this process and use of the software dongle that allowed the access of RES2DINV inversion software.

Special thanks to Akili Minerals Services directors: Dr. Cedric Simonet and Mr. Tom James first, for allowing me to start and finish my degree while still employed full time, second for allowing me to use company data for my thesis and reviewing and correcting my thesis through the process.

I would like to especially thank my family whose support and encouragement helped keep me focused, worry free and have carried me through this process.

To my friends and fellow graduate students, I thank you for your friendship, encouragement and support.

A very special thank you to Esther Kananu, You always prayed for me, believed in me, encouraged me, and inspired me to be the best man I can. Thank you so much.

Thanks to you all!!!!

TABLE OF CONTENTS

DECLARATION	i
ABSTRACT	ii
ACKNOWLEDGEMENT	iii
TABLE OF CONTENTS	iv
List of Figures.	vi
List of Tables.....	viii
Acronyms.....	ix
1. CHAPTER ONE: INTRODUCTION	1
1.1. Background information	1
1.2. Problem statement	3
1.3. Aim and Objectives	4
1.4. Justification.....	4
1.5. Significance.....	5
1.6. Literature review	6
2. CHAPTER TWO: STUDY AREA	10
2.1. Location	10
2.2. Climate	11
2.3. Vegetation	11
2.4. Land use and Land Resources	11
2.5. Physiography and drainage.....	11
2.6. Geology and Structures.....	12
2.7. Soils.....	16
2.8. Surface and Ground Water Resources.....	16
3. CHAPTER THREE: BASIC PRINCIPLES.....	18
3.1. Induced Polarization	18
3.2. Resistivity.....	26
3.3. Inversion	30
4. CHAPTER FOUR: MATERIALS AND METHODS.	33
4.1 Materials	33
4.2 Methods.....	36
4.3. Quality control (QC)	38

4.4.	Data transfer, processing and interpretation.....	38
5.	CHAPTER FIVE: DATA ACQUISITION.....	39
5.2.	Field procedures.....	40
5.3.	Typical daily Schedule.....	40
5.4.	IP/Resistivity gradient.....	41
5.5.	IP/Resistivity Pole-dipole.....	42
6.	CHAPTER SIX: DATA PROCESSING.....	44
6.1.	Data processing.....	44
6.2.	Results.....	47
6.2.1.	Gradient maps.....	47
6.2.2.	Pole Dipole Pseudo sections.....	50
6.2.3.	Inversion models and Interpretation.....	55
7.	CHAPTER SEVEN: DISCUSSION, CONCLUSION AND RECOMMENDATIONS.....	65
7.1.	Discussion.....	65
7.2.	Conclusion.....	67
7.3.	Recommendations.....	69
8.	REFERENCES.....	70

List of Figures.

Figure 1-1: Satellite Image of the study Area	2
Figure 2-1: Location of Kamwango.	10
Figure 2-2: Regional Geology of the study area.....	13
Figure 2-3: Geology of the wider Kamwango area	15
Figure 2-4: Mapped QV's, previous drill holes and some results	16
Figure 3-1: A conventional array with four electrodes showing the current and potential dipoles	18
Figure 3-2: Graphs of the source current and measured voltage and chargeability equation.	19
Figure 3-3: IP values for some Rocks and Minerals	20
Figure 3-4: Electrode polarization illustration 1	21
Figure 3-5: Electrode polarization illustration 2	22
Figure 3-6: Membrane polarization illustration 1.	22
Figure 3-7: Membrane polarization illustration 2.	23
Figure 3-8: Membrane polarization illustration 3	23
Figure 3-9: Illustration of the second form of membrane polarization.....	24
Figure 3-10: Current point source in an infinite medium.....	26
Figure 3-11: Lower hemisphere of an enclosed earth.	27
Figure 3-12: Two point sources of current on surface of homogeneous ground.	28
Figure 3-13: Opposite polarity of the two point sources	28
Figure 3-14: Resistivity of rocks soils and Minerals.....	29
Figure 3-15: Graph of data misfit against model norm.	32
Figure 4-1: Zonge GGT-3 time domain transmitter.	343
Figure 4-2: Zonge VR1B voltage regulator.....	354
Figure 4-3: Honda GX 240 3 phase generator.	354
Figure 4-4: Zonge GGT-3 geophysical transmitter and Single core, multi-strand steel wires on reel	35
Figure 4-5: Scintrex IPR12 Receiver.....	375
Figure 4-6: Typical four electrode array.....	37
Figure 5-1: Kamwango grid.	39
Figure 5-2: Illustration of current line arrangement.....	41
Figure 5-3: Side and plan view of the Gradient array.	42

Figure 5-4: Illustration of pole dipole array	43
Figure 6-1: Pole Dipole data in text format.	46
Figure 6-1: Chargeability anomaly profile map.....	48
Figure 6-2: Resistivity anomaly profile map.....	49
Figure 6-3: L 500E.....	50
Figure 6-4: L 600E.....	51
Figure 6-5: L 900E.....	51
Figure 6-6: L1000E.....	52
Figure 6-7: L1100E.....	53
Figure 6-8: L1900E.....	53
Figure 6-9: L2000E.....	54
Figure 6-10: L 500E Mx and Rho inversions and Interpretation.	56
Figure 6-11: L 600E Mx and Rho inversions and Interpretation.	57
Figure 6-12: L 900E Mx and Rho inversions and Interpretation.	58
Figure 6-13: L 1000 Mx and Rho inversions and Interpretation.....	59
Figure 6-14: L 1100 Mx and Rho inversions and Interpretation.....	60
Figure 6-15: L 1900 Mx and Rho inversions and Interpretation.....	61
Figure 6-16: L 2000 Mx and Rho inversions and Interpretation.....	62
Figure 6-17: Plan view map of the Model interpretations.	63
Figure 6-18: Figure 6-17 superimposed on the geological map	64
Figure 7-1: Location of nine proposed boreholes.	68

List of Tables

Table 3-1: Chargeability of materials with charging and integration times of about 1 minute each.....	25
Table 3-2: Chargeability of materials with charging and integration times of 3 seconds and 0.02-1.0 seconds respectively.....	25
Table 3-3: Chargeability of minerals at 1% concentration in the samples.	25

Acronyms

IP & R	Induced Polarization and Resistivity.
Rho/ ρ	Resistivity.
ρ_a	Apparent resistivity.
AMS	Akili Minerals Services Ltd.
Mx/ M	Chargeability
Ma	Apparent chargeability.
mv/v	millivolts per volts.
PFE	Percentage Frequency Effect.
SIP	Spectral Induced Polarization.
MF	Metal Factor.
$\Omega.m$	Ohm meter.
1D, 2D, 3D	1, 2 and 3 Dimensions.
FEM	Finite Element Method.
BIF	Banded Iron Formation.
QV	Quartz Veins.
GPS	Global Position System.
UTM	Universal Transverse Mercator

1. CHAPTER ONE: INTRODUCTION

1.1. Background information

Kamwango, herein, referred to as the study area, is located about 6 km from Rongo town along Rongo-Rangwe road in Migori County, Kenya (figure1-1). It covers approximately 4 square kilometer and is administratively situated in the East Nyokal (Kamagambo) location. The rocks in the area are Archaean in age and are known as the Migori greenstone. The area mostly comprises of Archaean age metavolcanics of the Nyanzian system. Migori area, which is in the region and located south west of the study area (figure 1-1), has previously recorded production of gold and is home to one of Kenya's oldest gold mine.

According to African Queen Mines (Once a license holder in the area), it is reported that gold was discovered in the area by a farmer who unsuspectingly found a gold nugget in the soil. This resulted in encroachment by artisanal miners who have since then been recovering gold from quartz lag on the surface and quartz vein pebbles in the top soil. Currently, mining is a major economic activity and source of livelihood for the locals. Recent studies by African Queen Mines show the presence of a layer below the topsoil in the area which is highly mineralized with gold. Mineralization is in sheet swarms and stockworks of gold bearing quartz veins with the gold being associated with pyrite, galena and other sulphides.

IP and Resistivity are some of the geophysical methods used for mapping this kind of mineralization for cost effective drilling programs (significant cost reduction during the drilling phase) as they contribute to better defined targets. Since target detection is usually very difficult when using only one geophysical method, both IP and resistivity data were acquired simultaneously with the same instrument to detect the desired target and enhance interpretation of observed data.

Inversion of these data enables the geophysicist to visualize and get more insights of the subsurface by conversion of observed data into images of the subsurface. The inversion process seeks to produce 1D, 2D or 3D distribution of the physical properties that explain acquired field measurements. With the advancement of inversion programs such as RES2DINV of Geotomo, DCIP2D of UBC and Voxi of

Geosoft, and fast computers, modeling is faster, more reliable and can be used to generate targets confidently.

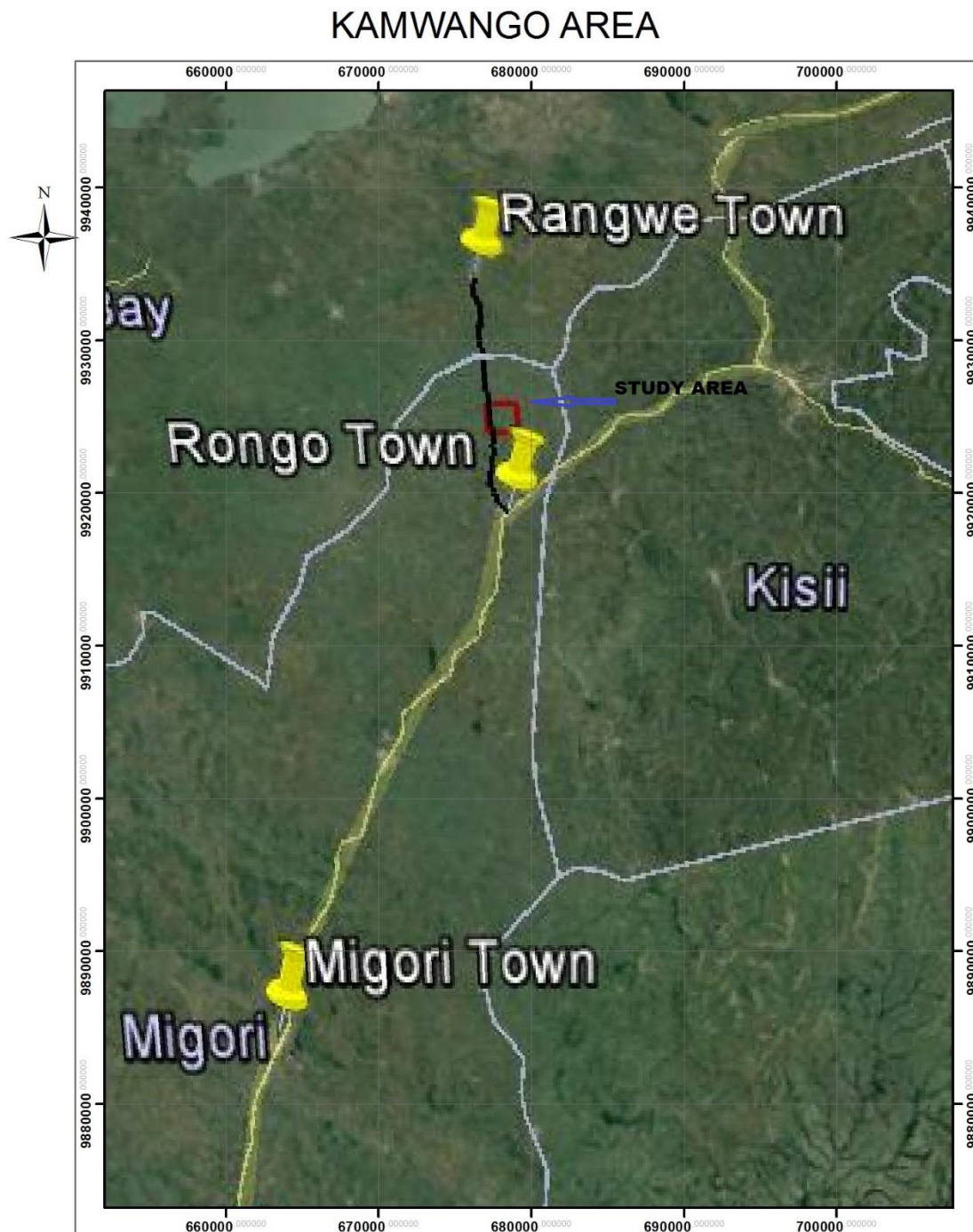


Figure 1-1: Satellite Image of the study Area

1.2. Problem statement

In Kamwango, the potential for gold is seen by the numerous artisanal workings in the area. A total of 12 big and small workings are active in the area, the biggest being at farm 2 and Komito mine where artisans are mining the gold from quartz lag in the topsoil. The presence of this quartz lag mineralization could indicate a widespread vein system. Previous work done by the license holder including geological mapping, sampling, pitting and trenching showed a highly gold-mineralized layer below both the topsoil and the overburden covering the area and extending out, with visible gold present in significant quantities. Several test drill-holes were done to intersect previously mapped structures, which trend NW and NE, exposed by artisanal workings above them (Figure 2-4). The results of the test drill holes revealed the presence of a highly auriferous mineralization near the surface, in Kamwango.

These findings prove that the area has potential necessitating more work to be done to develop an expanded drill program. The work will be important to better define the mineralized zone intercepted in the previous drill holes as well as look for new drilling targets in the area. There is, therefore, a need to carry out an intensive geophysical survey over the area and use data processing techniques that enhance interpretation in order to identify suitable drilling sites.

IP and Resistivity are some of the most effective geophysical methods to map this kind of mineralization. The advancement in inversion programs allow for a more definitive interpretation that produces more realistic and reliable outputs, reducing costs and minimizing risks before deciding to drill.

1.3. Aim and Objectives

Aim:

The aim of this research is to conduct IP and Resistivity survey in the search for possible gold mineralization in Kamwango area, interpret the data and delineate follow-up drill targets.

Objectives:

- To map possible gold mineralization using IP and Resistivity methods.
- To use advanced processing techniques to process the data, correlate them with other available geological information and interpret the results.
- To locate drill hole targets for follow-up from the interpreted results.

1.4. Justification

Kamwango has potential for gold evident by the extensive artisanal workings in the area. The results of previous work done in the area, which include: geological mapping, pitting, trenching and soil sampling, delineated a smaller target for follow up using geophysical methods. Some of the preliminary drill-hole test done by the license holder returned quite significant assay results. The results show that the area has great potential for gold. Available data and information from the area are, however, not sufficient for one to make reliable and cost effective decisions on where to drill for better resource definition.

Geophysical processing and interpretation techniques are an integral part of the geophysical exploration process. Due to limited resources, there is a need to have techniques that efficiently analyze, integrate and strategically use the geophysical data. The techniques must be able to mitigate the high costs and be efficient to increase confidence when making decisions. The demand for innovative solutions in processing of the data is, therefore, strong especially in search for deposits within complex and challenging subsurface environments.

1.5. Significance.

The research will be a significant endeavor in providing results that will help delineate targets for drilling which will, in turn, help define the gold resource in the study area. Given the high economic value of gold, the study has the potential to bring a positive economic effect on the local community.

This research will also help save money for an investor as it utilizes effective geophysical processing techniques allowing better interpretation, producing reliable follow-up targets, focusing exploration projects and, therefore, significantly reducing costs during the drilling phases. In the best cases, a 2D IP program costing something in the order of magnitude of a few tens of thousands of dollars will save a few hundreds of thousands of dollars' worth of drilling by narrowing the size of targets.

Lastly, the results from this research will serve as a future reference for researchers on the subjects of IP and Resistivity surveys for gold mineralization in the study area and educate mining investors on the potential of the study area.

1.6. Literature review

1.6.1. Gold aspects and mineralization.

Gold has been mined in western Kenya since pre-colonial times. In the Migori segment, in south western Kenya, gold mineralization occurs along a system of veins, mostly quartz, which, in some places, has proportions of pyrite, arseno-pyrite, chalcopyrite and galena. The quartz veins occur as impregnation in host rocks such as BIF or mafic volcanics, (Schluter, 1997). According to Barnes (1961), two types of quartz are apparent, a barren, glassy, white quartz and a gold bearing darker milky quartz. Earlier studies by Shackleton (1946), deduced that the area consisted of sulphide replacement veins. The rocks in the vicinity have a regional foliation trending west-north-west and steeply dipping to the north or south.

Ichangi (1993), concluded that the belt is a Zn-Cu-Au-Ag massive sulphide deposit, with numerous gold occurrences restricted to the greenstone belt. According to him, a considerable economic potential of gold exists in the Migori area as the type of gold mineralization, volcanogenic massive sulphides, is the most common and widespread in other Archean cratons.

According to African Queen Mines, 2010, the main type of mineralization in Kamwango and the surrounding area comprises, sheet swarms and stockworks of gold-bearing quartz veins commencing at or near the surface. The gold is typically associated with pyrite, galena and other sulphides. Shear zone related structures mapped in the area may have played a role in the location of the gold bearing quartz veins.

1.6.2. Induced polarization

Induced polarization (IP) was first developed in 1920 by Conrad Schlumberger (Schlumberger, 1920). After terminating a direct current that he had fed into the ground, he observed a decay in voltage. He attributed this phenomenon to electrical polarization and used it to locate unexplored ores. His research on IP was discouraged due to background noise which overshadowed the IP effect. Sumner (1976) did research in the Soviet Union in the 1950's on the use of IP in petroleum well logging and since then it has been used as a prospecting technique. Extensive research has been done on the application of IP in various fields. For instance,

Vacquier et al. (1957) and Marshal and Madden (1959) studied the application of IP in hydrogeology Towel et al (1985) studied the application of IP in environmental studies and Sterberg and Oehler (1990) studied the application of IP in oil and gas exploration.

Induced polarization is an extremely complex electrochemical phenomenon and is yet to be fully understood. However, Siegel (1959), Keller and Frischknecht (1966), Sumner (1976), Telford et al (1990) and Zhadanov and Keller (1994) have contributed valuably to the description of the IP effect.

1.6.3. Resistivity

The method was first developed in 1912 by Conrad Schlumberger and since the 1970s it has been widely used in the assessment of ground water, mapping of geological structures and search for conductive ores (Reynolds, 1997).

1.6.4. The inverse problem

Inversion, as a process seeks to produce 1D, 2D or 3D distribution of the physical properties that explain acquired field measurements. This process is not unique, meaning that a single dataset may result into numerous models that acceptably explain it (Aiken et al, 1973), (Dwain, 2005). Therefore, to validate the inverse model, an experienced interpreter and information from geological studies on the area is important. The interpretation process is intertwined with the inversion process to ensure best results.

Before solving the inverse problem, it is important to understand the forward problem which is the process of computing a response from a given model (Oldenburg and Li, 2005). It is a straight forward and simple concept because you only expect one answer from its calculation.

When determining the value of a given survey, forward modeling is one of the important step. When designing geophysical surveys, it helps in making wise exploration decisions (Mufti 1976, 1978).

. In geophysical surveys, forward modeling is a process which involves first understanding the sought target, secondly, creating a hypothetical model from which

the response of different survey types is computed. It is easy to clearly see the sought targets in some surveys while it is not in others

Inverse problem is the reverse of the forward problem; instead of finding one result to a specific model, inverse modeling helps show which best fit model results from acquired field data. The problem is non-unique because many models can result from the same surface data. Imposing independent constraints from other geological surveys can help mitigate the non-uniqueness problem.

The inverse problem question is how to get results that represent the subsurface from the observed data. Other sources of information such as drill data, lithology, and thickness of overburden and assay results from drilling are the answer to this question. The inverse problem is constrained to only a small number of models that can possibly result from the data by this information. These limited models have common traits that helps in making interpretations that align with other sources of information. Fast computers and algorithms play a big role on progress made in geophysical exploration inversions since the best models result from experiments or tests carried out in the model space by testing different environments with the different constraints from other geological information. These algorithms will either involve improved pseudo-section concepts (Loke and Barker, 1995) or computer – intensive resistivity inversions (Li and Oldenburg, 1994). Moreover, reliability of final models is improved by the ability to use other geological information to better direct the inversion process.

Several papers have been written on algorithms to carry out inversions of IP/Resistivity data, these include:

- Tsourlos (1995) - Finite Element Method (FEM) scheme- it's applied in the calculations of forward.
- Loke and Barker (1996) - the two developed an algorithm that didn't rely on the resistivity case.
- McGillivray and Oldenburg (1990) on the adjoint equation approach- when necessary, adding the equation into FEM scheme, helps solve the Jacobian matrix J (the divergence of the observations in respect of changes of the model's resistivity).
- Li and Oldenburg (1994) on DCIP2D- this is an inversion program which uses numerical solutions on over-parameterized and constrained optimization

problems to estimate chargeability and/or resistivity distribution in the subsurface.

2. CHAPTER TWO: STUDY AREA

2.1. Location

The study area is located about 380 km from the capital city of Nairobi by road and about 60 km north of the Tanzanian border. It forms part of the greenstone belt around Lake Victoria which is rich in gold. The belt extends to Tanzania and hosts known world-class gold deposits. These deposits include those at: Acacia mining's North Mara Mines and Bulyanhulu, which is about 100 km from the study area, and AngloGold Ashanti's Geita Mine (figure 2-1). The study was carried out in a 12 km² property owned by Stockport Exploration, a Canadian firm listed in the Canadian stock exchange.

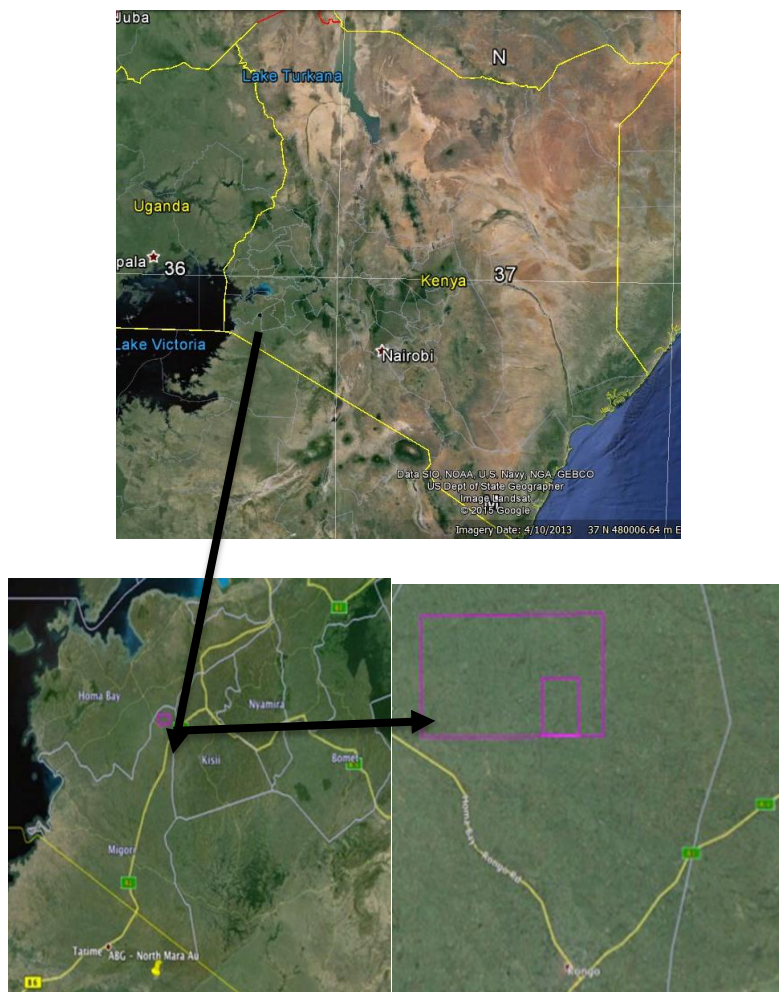


Figure 2-1: Location of Kamwango (Source: Google Earth).

2.2. Climate

Meteorological data for the area are available from Asumbi Mission, Marinde and Kamagambo. From the mean monthly rainfall of these stations, the mean annual rainfall is about 1550mm. From the rainfall distribution throughout the year; the area has two rainy seasons with a clear peak in March-May with April being the wettest month with a mean rainfall of about 250mm. The second but minor peak occurs in September-October with about 130mm per month.

The mean annual temperature is about 23°C with the driest months being January and February.

2.3. Vegetation

The vegetative cover in the study area is rich in both wild plants and food crops. Maize, sugarcane, finger millet, beans, cassava and sweet potatoes are grown as food and cash crops in the farmlands. Natural vegetation of scattered shrubs and acacia species and grassy fields has been cleared for human economic advancements. Traces of these can, however, be seen in the farm and homestead hedges. Natural trees also occur for both timber and fruits.

2.4. Land use and Land Resources

The land is subdivided into small pieces and the major land uses include small scale farming mainly rain-fed. The main crop is sugarcane which is sold to nearby sugarcane milling companies. The rest of the land is covered with pasture for livestock and infrastructure including human settlement, schools and access roads. Most locals are involved in artisanal mining which is a major source of income in the area.

2.5. Physiography and drainage

The project area is generally flat to very flat undulating slope. The altitude ranges from 1275m to 1400m above sea level. The main drainage channel in the wider Rongo area is River Kuja. However, the study area has smaller rivers like Riana, Misadhi, Aora Nam and streams where most of the surface runoff drains to.

2.6. Geology and Structures.

2.6.1. Regional Geology

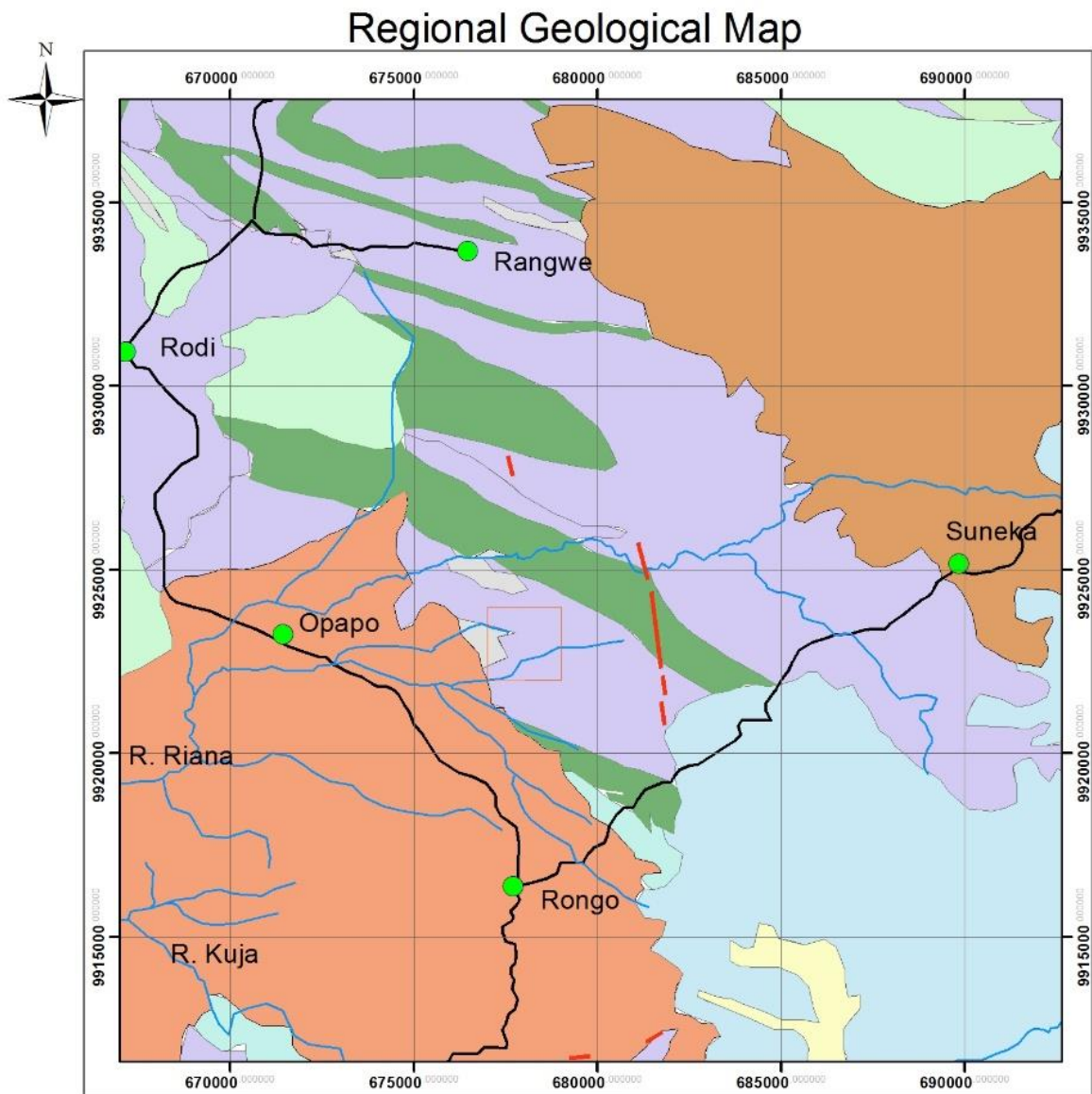
Geological study of the area and wider Kisii district was first carried out by Huddleston (1951) who made a geological map of the Kisii district in the late 1940's (figure 2-2). According to him, the area lies within the Migori greenstone belt which runs W-NW to E-SE between Lake Victoria and the Great Rift Valley. The belt is squeezed between the Migori Granite batholith to the south and a felsic volcanic succession to the north. Geology of the area consists of Archean greenstone belt that surrounds Lake Victoria. The Archean rocks are principally of the Nyanzian system, Kavirondo system and the Post-Kavirondo granites.

2.6.1.1. The Nyanzian System.

The Nyanzian system comprises generally a typical greenstone belt assembly of metamorphosed volcanics, sediments and granites. Its thickness has been estimated at about 7500m (Grantham et al, 1945). In Kenya, the system is composed of high proportions of sedimentary rocks, including slates, greywacke and conglomerates (Shackleton, 1964).

Recently, Ogola (1987), Akech (1988, 1991), Ichangi (1991, 1993) and Ngecu and Gaciri (1995) have contributed valuably to the systems lithology, structures, metamorphism and mineralization.

The system can be geographically divided into a northern and southern terrain. The main occurrence of the northern terrain is to the western side of Maseno where a sequence of volcanics from dacites to rhyolites through basalts and andesites can be seen (Akech, 1993). The southern terrain is represented by the Migori segment, which is in an almost linear contact to the Proterozoic Migori granite and trends in a WNW-ESE direction. At the base the segment is composed of BIF and mafic volcanics while at the top, the succession is overlain by intermediate to felsic volcanics with andesite tuffs interbedded with sedimentary rocks.



Legend

- | | |
|---|---------------------------------|
| Study Area | Kavirondian Conglomerates_Pro |
| Town_Project | Nyanzian, Kitere Granite_Proje |
| River_Project | Nyanzian, Rhyolites & dellenite |
| Road_Project | Post-kavirondian, minor intrus |
| porphyritic & non-porphyritic felsites & andersites | PostNyanzian, Diorite-porphyr1 |
| younger granites | Tertiary Nephelinites, Napheli |
| Basalt with minor mudstones_Pr | Andesites & dacites |
| Bukoban, Basalt_Project | Quartz veins |

Figure 2-2: Regional Geology of the study area (Huddlestone, 1951)

2.6.1.2. Kavirondian System.

The Kavirondian lies to the north of Kavirondo Gulf in Kenya (Hitchen, 1937; Stockley, 1943) and its rocks cover an area of about 6000 km² extending from the slopes of Nandi hills to Yala town. The system is composed of conglomerates, sandstones and mudstones and overlie the Nyanzian rocks unconformably.

Post Kavirondian granites occur as batholithic masses or stock-like bodies. Minor mafic intrusives composed of dolerites, gabbros and diorites which occur as dykes precede emplacement of the granites. Tertiary volcanics are composed of phonolite and alkaline lavas and carbinatites.

2.6.2. Local geology, Mineralization and structures.

The area is generally covered with a layer of overburden and topsoil and few rock outcrops are visible. Artisanal miners have been mining gold in the overburden and topsoil only and recover the gold in the soil profile from pebbles of quartz veins.

Earlier pitting, trenching and sampling by African Queen Mines show a layer below the overburden which is highly mineralized with gold with the gold being visible in some areas. Generally, rocks in the area range from mafic to intermediate metavolcanics which are often silicified and epidotised extensively. Mainly, the areas mineralization is composed of near surface stockworks of quartz veins bearing gold and sheetswarns. Gold mineralization is associated with sulphides such as pyrites and galena. According to the licence holder, grab samples collected from historic artisanal workings have given gold results ranging from 2 g/t to as high as 96 g/t. In the western parts, geologic exposures reveal late stage granites in the area, mafic and felsic volcanic rocks in the central and eastern areas and structures related to shear zone, which have certainly contributed to the location of the quartz veins which have gold (figure 2-3).

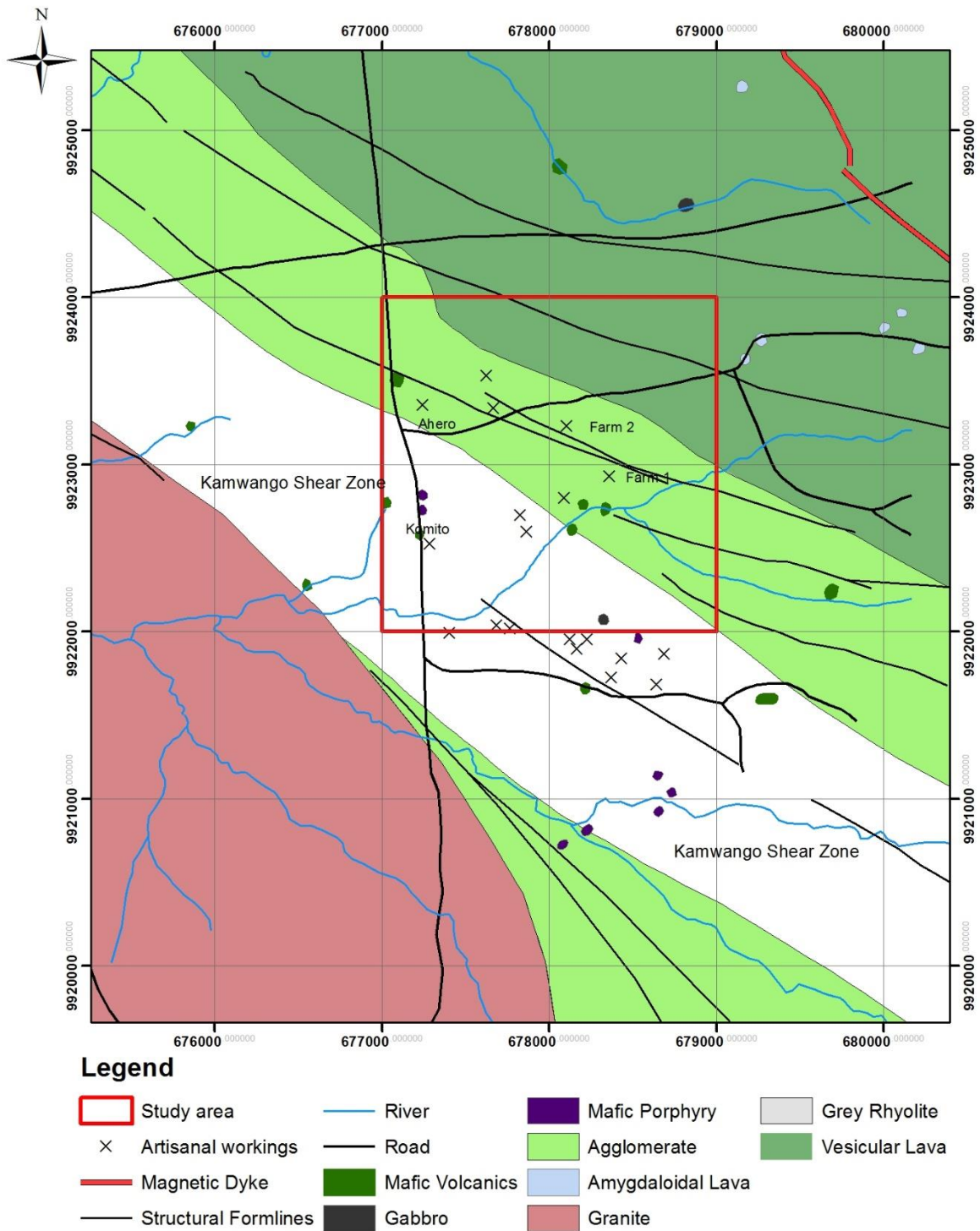


Figure 2-3: Geology of the wider Kamwango area (Source: David Ndago) (Personal communication)

Figure 2-4 shows known quartz vein structures trending NW- SE. the veins were mapped on some of the exposed artisanal workings in the area. Previously drilled holes were designed to intersect the quartz veins.

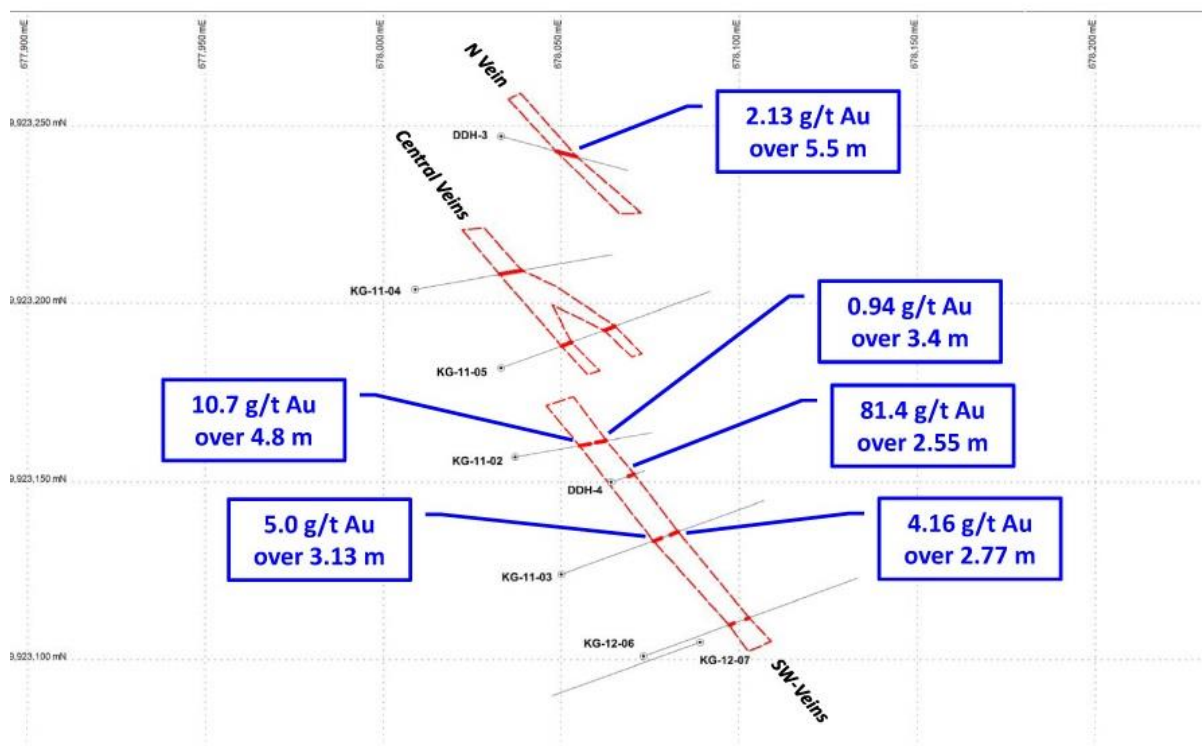


Figure 2-4: Mapped QV's, previous drill holes and some results (Stockport Exploration)

2.7. Soils

The soils in the area can be considered to range from excessively drained stony and rocky soils which are poor for farming to well drained shallow to moderately deep, very dark grey clay loam which is good for farming. In some other areas, the soils are disturbed due to the numerous tailing dams from the artisanal mining.

2.8. Surface and Ground Water Resources

The main water source for most activities in the area is River Riana which is one of River Gucha's tributary, and originates from the Kisii Highlands. Springs and shallow wells also add to the available water resources in the area under study. Protected

springs offer good quality water but consumers have to get it from the point of supply.

The wider Lake Victoria catchment basin is expected to recharge the deeper aquifers through seepage. The seasonal streams and the perennial rivers in the larger catchment area are excellent modes of groundwater recharge by either direct or by way of regional replenishment. The vegetative cover and low gradients encourage rainfall water infiltration and eventual percolation into the subsurface. The good soil cover by the foliage in the area is expected to maximize recharge. Direct recharge and lateral regional replenishment as a seasonal mode of recharge is expected to contribute highly to the ground water regime.

3. CHAPTER THREE: BASIC PRINCIPLES

3.1. Induced Polarization

IP is the measure of slow voltage decay in the ground after the current is switched off; in simple terms, it is the measure of the capacitance of the subsurface. The phenomenon occurs when an electric current passing through the ground is stopped, resulting to the observation of a potential difference which diminishes in a time dependent. The rate at which the above potential diminishes depends on the level of water saturation in the ground and pore geometry.

Two electrodes (current dipole) are used to introduce current in the ground, voltage builds up in the ground and is measured between two potential electrodes (potential dipole), (figure 3-1).

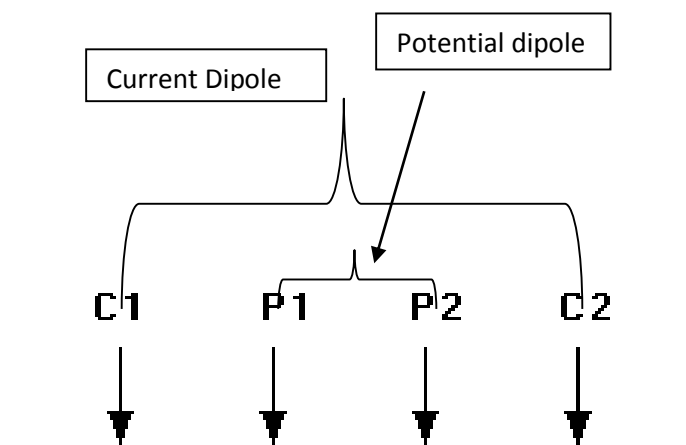
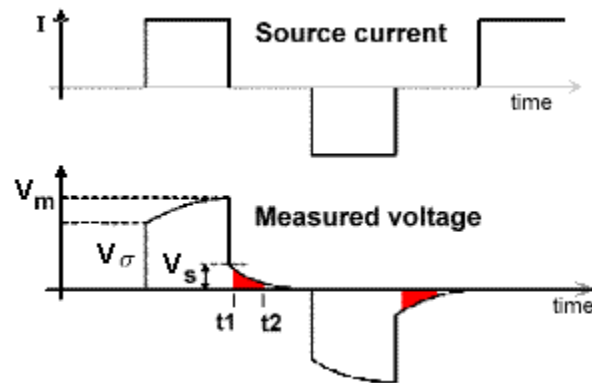


Figure 3-1: A conventional array with four electrodes showing the current and potential dipoles (Loke, 2015)

On switching off current at the source, the voltage measured at the potential dipole diminishes slowly with time (figure 3-2). Two types of voltage are observed, the primary voltage, which vanishes immediately the current source is switched off and

the secondary voltage which decreases with time in a material dependent manner (Sumner, 1976). Chargeability (M) is the term most commonly used to measure the degree of polarizing effect (Siegel, 1959) in time domain. It is the ratio of the overvoltage to the primary voltage and is expressed in millivolts per volt (mv/v) (Reynolds, 1997). Chargeability (M) is calculated from the area under the decay curve as shown in equation 3-1 below.



$$M = \frac{1}{V_m} \int_{t1}^{t2} v_s(t) dt \quad \text{-----} \quad 3-1.$$

Figure 3-2: Graphs of the source current and measured voltage and chargeability equation (Reynolds, 1997).

Measurement of the overvoltage is almost impossible at the time current is terminated due to an electromagnetic effect which, on switching, produces a transient disturbance. Therefore, there is a time delay between current cessation and start of measurement. After current cessation, decay is measured in several time windows then integrated to give the apparent Chargeability (Ma). Ma is expressed in milliseconds or millivolts per volt (Reynolds, 1997). Studying the form of overvoltage decay-curve can then give more detailed information about the IP characteristics. Field values are measured in apparent chargeability and are influenced by the volume of the earth and the array geometry (Butler, 2005).

IP is mostly suited in disseminated metal sulfide ores prospecting because of their strong IP-effect and is suitable to be used together with resistivity methods

(Reynolds, 1997). The disseminated nature of these deposits makes it difficult to be detected using standard resistivity due to the frequently low resistivity contrast.

The other most common sources of strong IP-effect is clay, it is therefore, important to have more geological information of an area to accurately tell the source of the IP-effect. Figure 3-3 below shows chargeability ranges for different materials.

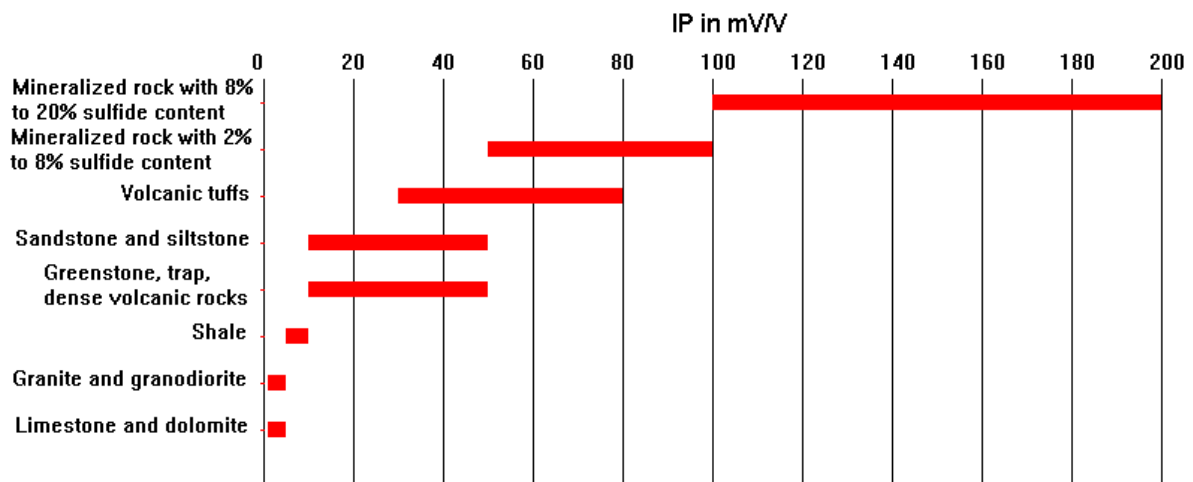


Figure 3-3: IP values for some Rocks and Minerals (Loke, 2015)

From figure 3-3 above, IP effect due to electrode polarization with values ranging from 100-200mV/V for example in sulfide mineralization is much larger than that due to membrane polarization for example in clay minerals.

IP effect can also be measured in frequency domain observations. Measurements are made at two different frequencies, apparent resistivity at high frequency and apparent resistivity at low frequency. The resulting parameter is known as the frequency effect. The measurement can be expressed as a percentage of frequency effect (PFE) (Wait, 1959) and can be expressed as equation 3-2:

$$PFE = 100 \left(\frac{\rho_{a2} - \rho_{a1}}{\rho_{a1}} \right) \quad \text{-----} \quad 3-2.$$

where ρ_{a2} and ρ_{a1} are apparent resistivity at high and low frequency respectively

Phase shift between the input current and the potential signal measured in milliradians is another measure of frequency domain IP

It is also possible to measure multi-frequency IP named Spectral IP (SIP) or complex resistivity (Reynolds, 1997). Recent research by Vanhal et al. (1992) has made use of the SIP method for contaminants detection in environmental surveys. Frequency-domain IP can also be expressed in terms of metal factor (*MF*) whereby a numerical multiplying factor places the *MF* in the same numerical range as resistivity and chargeability (Sumner, 1976). The *MF* parameter is given by *PFE* or *M* divided by the corresponding apparent resistivity. Plots of the parameter emphasize where both high resistivity and high chargeability exists or where there is significant occurrence of metallic mineralization. Metallic minerals, for example sulfides, are, however, often disseminated. More likely than not, the ore in this case will have a correlation of high resistivity with high chargeability, and for this reason *MF* is rarely used.

IP effect can be described in two mechanisms: one is the Electrode (grain) polarization or overvoltage, illustrated in figures 3-4 and 3-5, which, (where metallic minerals are present) is as a result of variations between ionic and electronic conductivity. It is generally larger in magnitude than the background IP and depends on the presence of metallic minerals in the rock/soil. Like the name suggests, grain polarization occurs when a pore or a small fracture in the rock is blocked by an electrically conducting mineral grain as shown in figure 3-4. When this happens, electrons will tend to accumulate on one side of the grain. When a current is transmitted, the grain is polarized. Voltage decay is observed when the current is switched off as a result of ions diffusing back through the electrolytic medium, which gives the induced polarization effect (Parasnis, 1966).

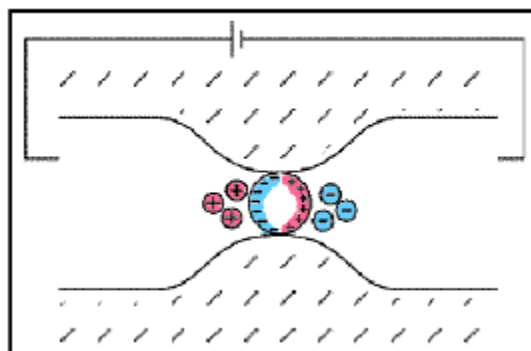


Figure 3-4: Electrode polarization illustration 1 (Bertin and Loeb, 1976)

Figure 3-4 above gives an illustration of pore space blocked by a metallic particle and charges accumulating when electric field is applied.

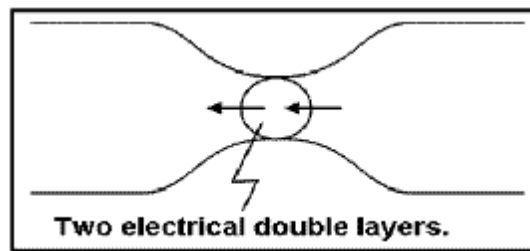


Figure 3-5: Electrode polarization illustration 2 (Bertin and Loeb, 1976)

Figure 3-5 above gives an illustration of two electrical double layers which add to voltages measured at the surface.

This mechanism will occur in materials with high conductivity such as sulfides, oxides and graphite. The IP-effect is higher in materials with a higher mineral content and surveys suggest that it is directly proportional to the resistivity of the host rock (Bertin and Loeb, 1976). Since electrode polarization is a surface phenomenon, it is inversely proportional to the metallic grain size and is, therefore, a suitable method in exploration of disseminated ore bodies.

Second is the Membrane or electrolytic polarization which is as a result of variation in the mobility of ions in fluids throughout the rock structure. It constitutes the background (normal IP effect) and may occur in rocks/soils which don't have metallic minerals. It is caused by either the shape of the pore channel or clay particle presence. In the first case, mineral surfaces attract positive ions from the pore fluid. Due to their negatively charged nature, this results in the development of thick positively charged layer on the surface. If the pore channel is narrower than this layer, a barrier to the negative ions is made of positive ions which also produce potential over the pore channel.

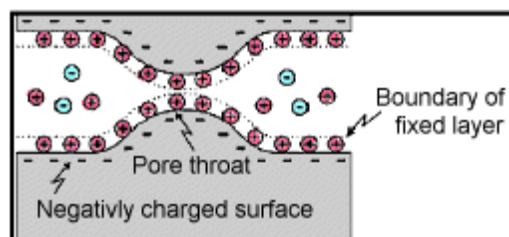


Figure 3-6: Membrane polarization illustration 1 (Bertin and Loeb, 1976).

Figure 3-6 above illustrates that membrane polarization results where pore space narrows to within several boundary layer thicknesses equal to the thickness of ions adsorbed to a surface.

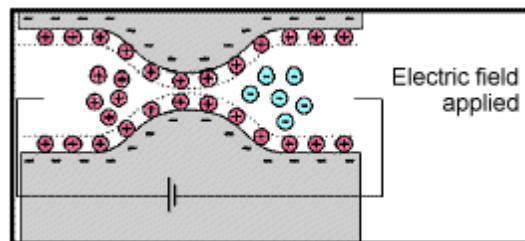


Figure 3-7: Membrane polarization illustration 2 (Bertin and Loeb, 1976).

The figure above illustrates that when pore space narrows, charges accumulate and cannot flow easily when an electric field is applied.

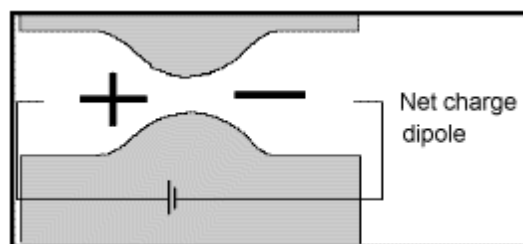


Figure 3-8: Membrane polarization illustration 3 (Bertin and Loeb, 1976)

The figure illustrates that the result (from figure 3-6 and 3-7) is a net charge dipole which adds to any other voltages measured at the surface.

In the second case, when clay particles are present in the pore spaces and the pore spaces are small enough to produce a barrier (Reynolds, 1997), negatively charged clay particles attract the positive ions and build barriers for the negatively charged ions.

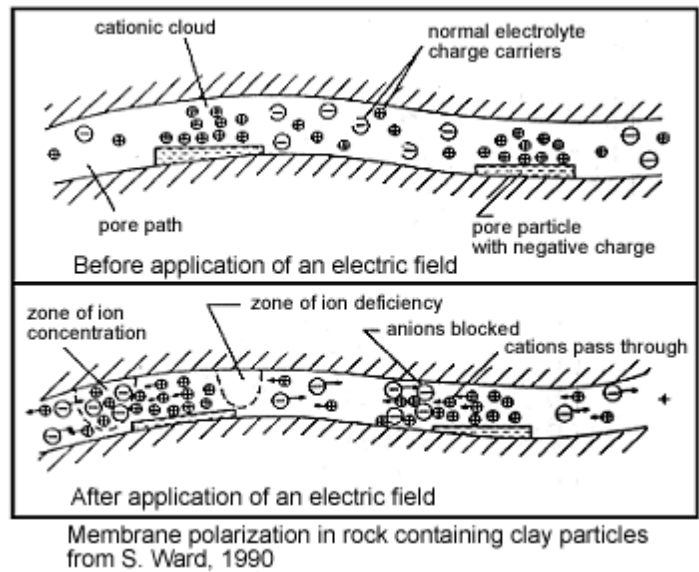


Figure 3-9: illustration of the second form of membrane polarization. (Bertin and Loeb, 1976)

This is a second form of membrane polarization similar to the first, where ionic solution paths are partially blocked by clay particles partially.

This IP mechanism tends to be inversely proportional to pore fluid ion concentration (Slater and Lesmes, 2002) ;(Bertin and Loeb, 1976). The two mechanisms have the same appearance on the IP decay curve though a higher contribution to the IP-effect is by electrode polarization (Bertin and Loeb, 1976).

Typical chargeabilities for materials

Telford et al, (1976) provided a general guide to possible chargeabilities of different materials. From the guide, it is observed that field measurements tend vary from laboratory values because in field measurements, large volumes of mixed materials are involved.

The examples (tables 3-1, 3-2 and 3-3) indicate that in determining the exact type of materials in the ground, it is difficult to use values of intrinsic chargeability (in models obtained by inversion of IP data) because a wide range of variability is to be expected.

Material type	Chargeability (msec.)
20% sulfides	2000 - 3000
8-20% sulfides	1000 - 2000
2-8% sulfides	500 - 1000
volcanic tuffs	300 - 800

sandstone, siltstone	100 - 500
dense volcanic rocks	100 - 500
shale	50 - 100
granite, granodiorite	10 - 50
limestone, dolomite	10 - 20

Table 3-1: Chargeability of materials with charging and integration times of about 1 minute each. (Telford et al, 1976)

Material type	Chargeability (msec.)
ground water	0
alluvium	1 - 4
gravels	3 - 9
precambrian volcanics	8 - 20
precambrian gneisses	6 - 30
schists	5 - 20
sandstones	3 - 12
argillites	3 - 10
quartzites	5 - 12

Table 3-2: Chargeability of materials with charging and integration times of 3 seconds and 0.02-1.0 seconds respectively (Telford et al, 1976)

Material type	Chargeability (msec.)
pyrite	13.4
chalcocite	13.2
copper	12.3
graphite	11.2
chalcopyrite	9.4
bornite	6.3
galena	3.7
magnetite	2.2
malachite	0.2
hematite	0.0

Table 3-3: Chargeability of minerals at 1% concentration in the samples. (Telford et al, 1976)

3.2. Resistivity

From Ohm's law $V = IR$ ----- 3-3.

Where V is the potential difference in Volts

I is the current going through the medium in Amperes

R is the resistance of current flow through the medium in Ohms

For a point source in an infinite medium, the resistance R and potential V are expressed as:

$$R = \rho \frac{L}{A} = \rho \frac{dr}{4\pi r^2} = \dots 3-4.$$

Where ρ is a constant of proportionality known as Resistivity

L is the length of the medium

A is the cross-sectional area of the medium

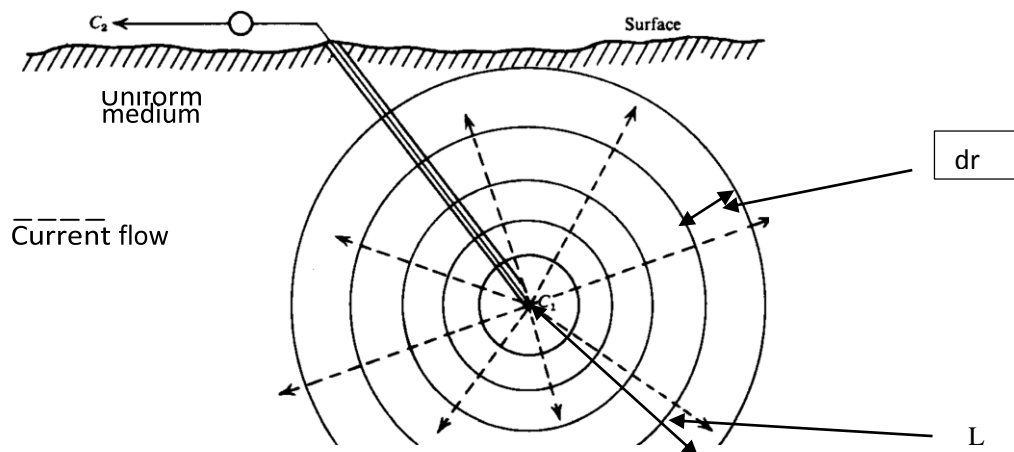


Figure 3-10: Current point source in an infinite medium (Dobrin, 1960.)

From eqn 3-3,

$$V = \frac{I\rho}{4\pi dr} \dots 3-5.$$

Therefore:

$$\rho = \frac{4\pi drV}{I} \dots 3-6.$$

This resistivity is called apparent resistivity. The apparent resistivity is equal to the real resistivity only when the material is uniform.

Most geophysical resistivity data is acquired on the surface of the earth, the air above the ground is an insulator (conductivity=0) and the current only flows in the ground. Therefore when calculating the current density in an equipotential sphere, the surface area becomes the surface of the lower hemisphere and the potential changes to:

$$V = \frac{I\rho}{2\pi dr} \text{ 3-7.}$$

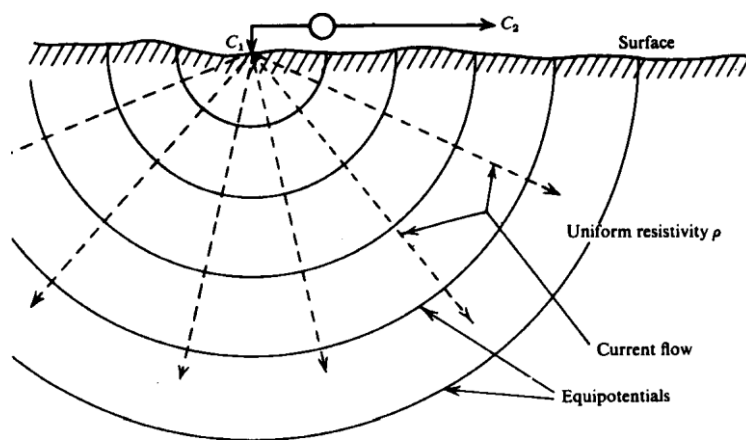


Figure 3-11: Lower hemisphere of an enclosed earth. (Dobrin, 1960.)

Practically field surveys measure the change in voltage between two electrodes not the potential itself. Therefore:

$$\Delta V = V_1 - V_2 = \frac{I\rho}{2\pi dr_1} - \frac{I\rho}{2\pi dr_2} \text{ 3-8.}$$

For the current to physically flow through the ground, we need two poles: the source and sink. Both poles generate electric potential but with opposite polarity.

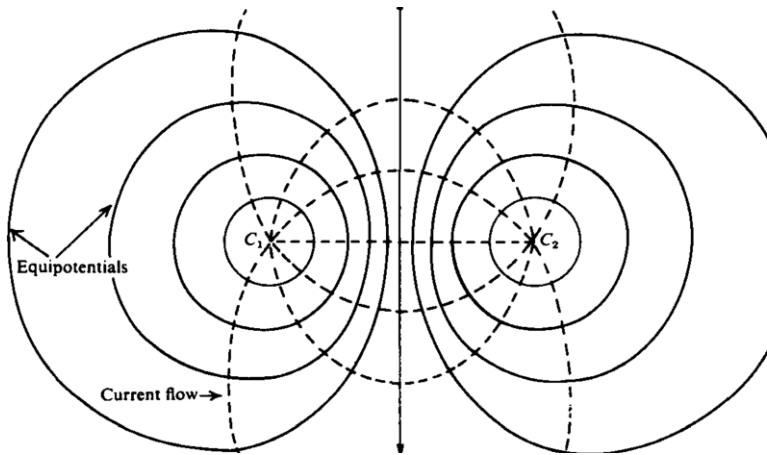


Figure 3-12: Two point sources of current on surface of homogeneous ground. (Dobrin, 1960.)

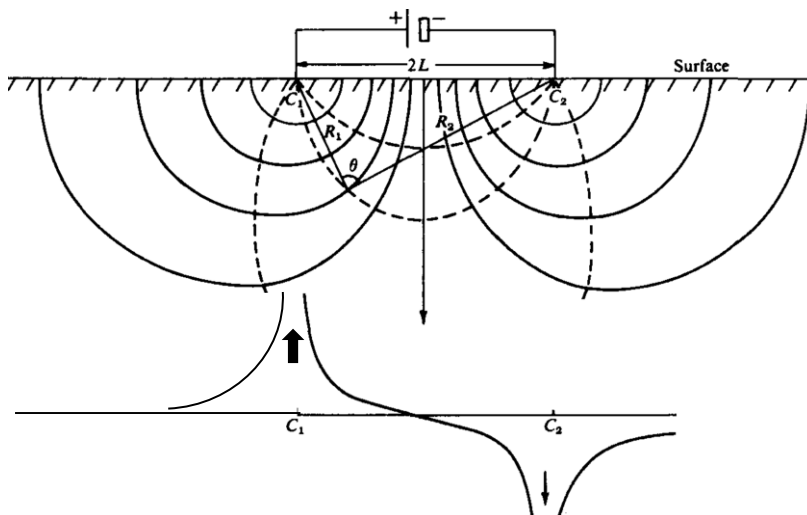


Figure 3-13: Opposite polarity of the two point sources. (Dobrin, 1960)

The total potential from the two poles is then:

$$V = V_1 + V_2 = \frac{I\rho}{2\pi dr_1} - \frac{I\rho}{2\pi dr_2} \quad \text{-----} \quad 3-9.$$

The total voltage between two points generated by the two poles is:

$$\begin{aligned} \Delta V &= \Delta V_1 + \Delta V_2 \\ &= \left(\frac{I\rho}{2\pi dr_1} - \frac{I\rho}{2\pi dr_3} \right) - \left(\frac{I\rho}{2\pi dr_2} - \frac{I\rho}{2\pi dr_4} \right) \\ &= \frac{I\rho}{2\pi} \left(\frac{1}{dr_1} - \frac{1}{dr_2} - \frac{1}{dr_3} + \frac{1}{dr_4} \right) \quad \text{-----} \quad 3-10. \end{aligned}$$

From the above equation then apparent resistivity becomes:

$$\rho_a = 2\pi \left(\frac{1}{r_1} - \frac{1}{r_2} - \frac{1}{r_3} + \frac{1}{r_4} \right)^{-1} \frac{\Delta V}{I} = K \frac{\Delta V}{I} \text{-----} 3-11.$$

where K is the geometrical factor which describes the geometry of the electrode configuration being used.

Resistivity of rocks, soils and ores types.

Typically, igneous and metamorphic rocks have higher resistivity values. According to Loke (2015), their resistivity is greatly dependent on the degree of fracturing and the percentage of the fractures filled with water. Quartzite, for example, has resistivity varying from 100 Ω.m to 100 million Ω.m (figure 3-14). A given rock can, therefore, have a wide range of resistivity depending on how dry or wet it is, an important characteristic in detecting weathering and fractured zones.

Sedimentary rocks have lower resistivity values due to their porous nature. Resistivity in this rock type is dependent on porosity and level of salinity of the water contained in the pores of the rocks.

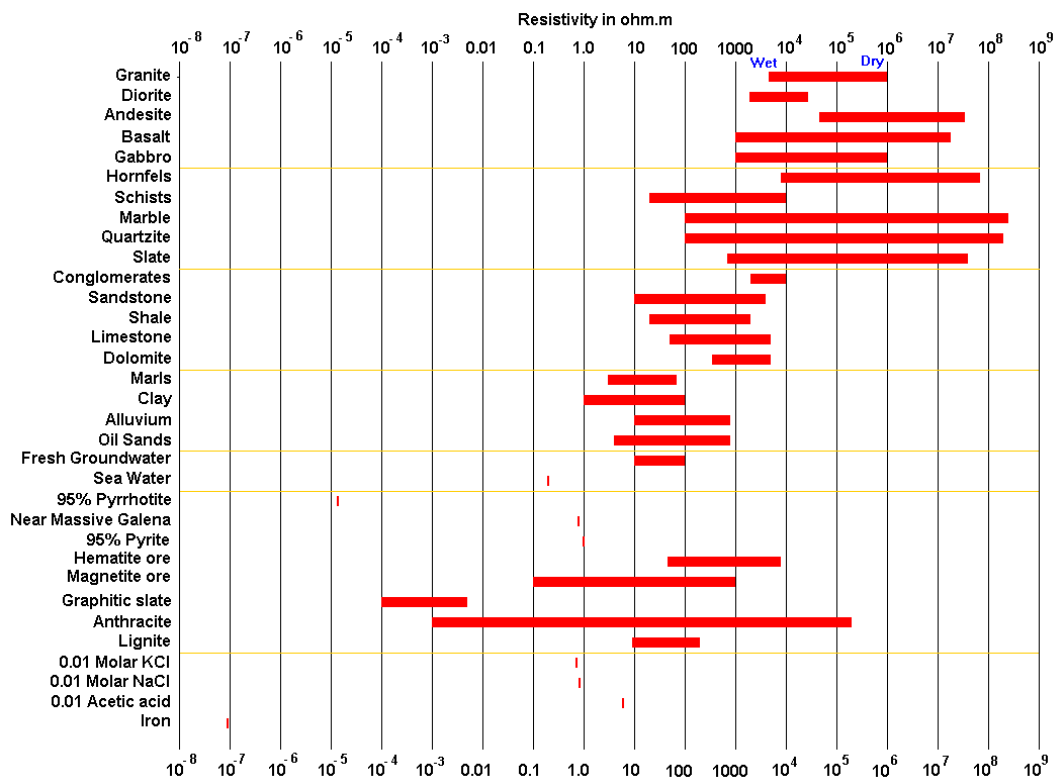


Figure 3-14: Resistivity of rocks soils and Minerals (Loke, 2015)

Resistivity of particular rocks and soils depend on several factors that include but not limited to the levels of salinity, degree of saturation and porosity. This is illustrated in figure 3-14 by the overlapping resistivity values of the different rock and soil types. From the figure, a big contrast between fresh ground water and sea water is noted. In this case, resistivity method would be an ideal technique to use in mapping the interface between saline and fresh water at the coastal areas (Gomez-Ortiz et al., 2007).

Metallic sulfides such as pyrite (which is associated with gold) typically have low resistivity values. These values and those of other ores vary depending on their nature (disseminated or massive)

3.3. Inversion

In forward process, you start with a particular model in the model space. This results is a particular observation in the data space. The inversion process is the opposite or reverse where you start with some observed data and you proceed backward to find the model that gives rise to the observation.

Practically, the observed data are not simply a point in the data space but a broader region due to observation errors.

Equations that guide the inversion

In the forward problem.

$$G[m] = d \quad \text{-----} \quad 3-12.$$

Here, we have some earth model m that is affected by some geophysical phenomena G that results into some observed data d

In the inverse problem.

$$G^{-1}[d] = m \quad \text{-----} \quad 3-13.$$

Thus, if we can find an inverse function G^{-1} and apply it to the earth model m to retrieve the observed data d , then the solution would be straight forward as the forward problem. However, G^{-1} does not exist hence the non-uniqueness. The inverse problem, therefore, becomes one of optimizing the closeness of a predicted

model and its forward calculated response to what we have observed and what we assume the model to look like.

We can quantify the closeness between the predicted model responses and our observed data with the following equations:

1. Data misfit

$$\Psi_d = \frac{1}{N} \sqrt{\sum_{i=1, N} \left(\frac{d_i^{obs} - d_i^{pre}}{\partial d_i} \right)^2}, \dots \quad 3-14.$$

When $\Psi_d=1$ \equiv "fits the data",

where,

d_i^{obs} – Observed data,

d_i^{pre} – Predicted model response,

The difference between the two, d_i^{obs} and d_i^{pre} is normalized by the error in the observed data ∂d_i . When the difference is equal to the error, i.e. $d_i^{obs} - d_i^{pre} = \partial d_i$. Then, $\Psi_d=1$ and the inversion fits the data.

2. The model norm which quantifies how close the predicted m_i^{pre} model is to a preferred reference m_i^{ref} model equation,

$$\Psi_m = \frac{1}{M} \sqrt{\sum_{i=1, M} \left(\frac{m_i^{ref} - m_i^{pre}}{\partial m_i} \right)^2}, \dots \quad 3-15.$$

Where,

m_i^{ref} - Reference model,

m_i^{pre} - Predicted model,

when $\Psi_m=0$ \equiv "conforms to geology".

The difference between the two is normalized by the error (confidence we have with the reference model) ∂m_i . When very confident with the reference model, we want the model norm to equal to zero meaning the inversion fits the geology very well.

Practically, we seek a model that satisfies the observed data and the known geology, so the inversion seeks to balance these two quantities before arriving at a final model. We can quantify this balancing act with the objective function:

$$\Psi_T = \Psi_D + \lambda \Psi_M, \quad \text{-----} \quad 3-16.$$

where, λ = regularization parameter that is adjusted by the inversion algorithm in successive steps. During each step calculation, the inversion tries to find a model that minimizes the objective function based on a condition that the data misfit is close to 1 (figure 3-15).

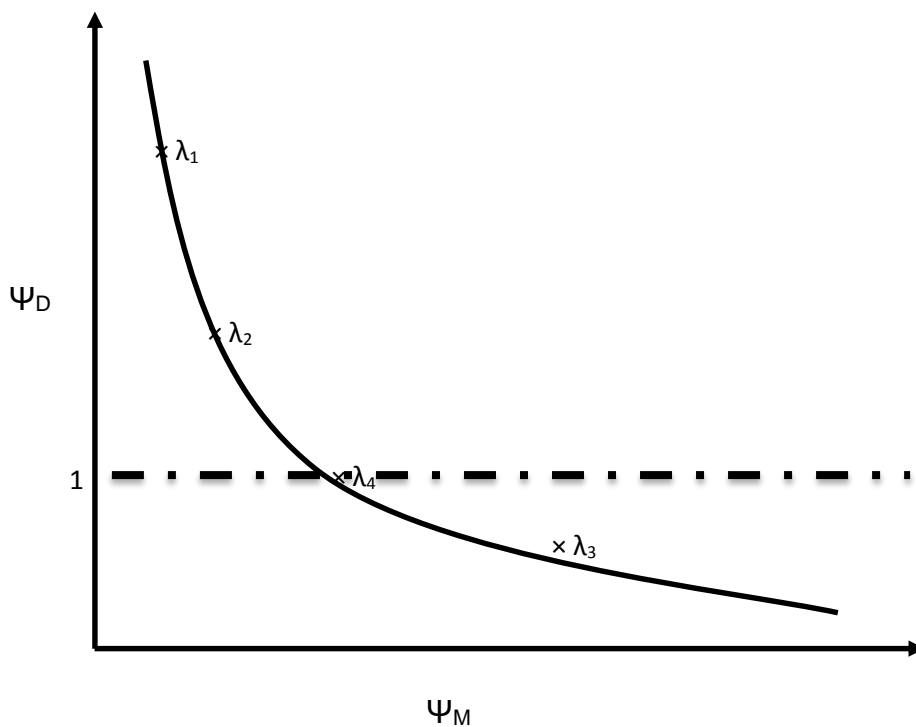


Figure 3-15: L curve of data misfit against model norm.

Each λ in figure 3-15 above represents iteration in the inversion, the final model is one that minimizes the objective function with the conditions that the data misfit is close to 1

4. CHAPTER FOUR: MATERIALS AND METHODS.

4.1 Materials

Before embarking on the field work, a desktop study was carried out. The study, included review of the Kisii geological map by Huddleston (1951) and other available geological information for the purposes of designing a sampling grid. The grid was designed in UTM locations which were later pegged in the field using a GPS unit.

For current transmission, the survey engaged the Zonge GGT-3 time domain transmitter (figure 4-1) powered by a Honda GX 240 3 phase generator (figure 4-2) which was regulated by a Zonge VR1B voltage regulator (figure 4.3). The transmitter is capable of putting out a square wave of 2, 4, 8 or 16 seconds 'on-off' time. The current output was accurately measured and monitored using a digital multimeter in the instrument.

Single core, multi-strand steel wires on reels were used for transmission of current from the transmitter to the current electrodes (figure 4.4). The electrodes were made of five steel rods, hammered into the ground and interconnected using a copper wire.



Figure 4.1: Zonge GGT-3 time domain transmitter.

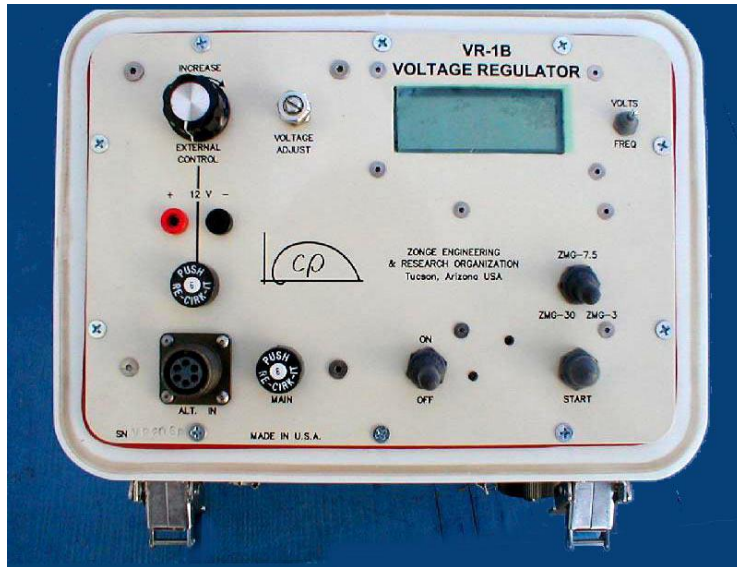


Figure 4-2: Zonge VR1B voltage regulator.



Figure 4-3: Honda GX 240 3 phase generator.

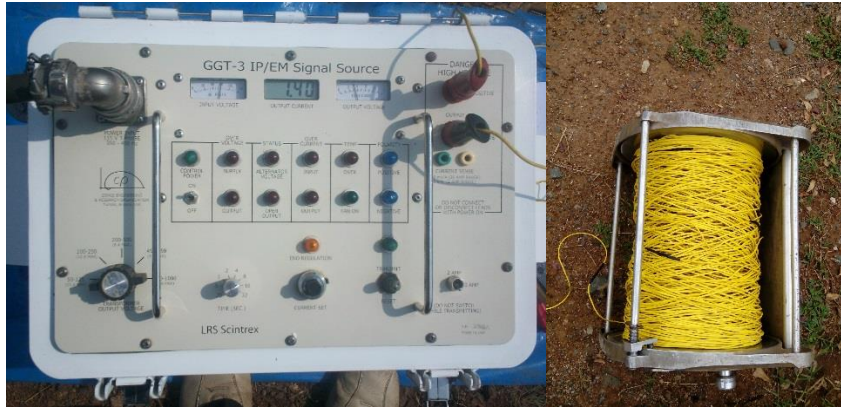


Figure 4-4: Zonge GGT-3 geophysical transmitter and Single core, multi-strand steel wires on reel.

For data acquisition, the survey utilized scintrex IPR-12 time domain receiver (figure 4-5). The unit operates on a square wave primary voltage and samples the decay curves at 14 gates or slices.

The receiver was connected to copper sulfate electrodes (non-polarizable porous pots) used as potential electrodes using multi electrode wires “snake wires” which terminated at each electrode’s location.



Figure 4-5: Scintrex IPR12 Receiver.

For communication, the survey engaged Motorola walkie talkies with a one way communication of one kilometer radius.

4.2 Methods.

The IP transmitter introduces direct current pulses into the ground through the current dipole (C1 and C2) (figure 4-5). The pulses are in 2 seconds “on-off” time duration. The current dipole is typically made up of two current electrodes. Current electrodes are physically represented by a group of stainless steel rods, which are hammered into the ground in a pit 0.5 – 1.0 m in diameter, equidistant from each other, and then interconnected with a thick copper wire.

The pit is dug with a mattock, then moistened with salted water for better conductivity. The idea is to introduce as much current as possible into the ground, so one should lower the contact resistivity as much as you can.

The IP receiver measures potential drop (voltage) in a potential dipole (P1 and P2) (figure 4-5) during the current transmission (“on-time”). The apparent resistivity value is calculated automatically based on the strength of the introduced current (I), the measured voltage (V_p), and the array coefficient, which depends on the mutual positions of C1, C2, P1, and P2. The receiver also measures the decay of the potential drop (induced polarization) in a potential dipole during the “off-time”; the chargeability value is automatically calculated as a ratio between the induced polarization measured during a specific part of the “off-time” (IP) and the initial voltage measured during the “on-time” (V_p).

Measurements of the potential drop are performed with the use of pairs of non-polarizable electrodes (porous pots filled with saturated solution of copper sulfate). The porous pots are put into shallow pits (5-15 cm deep), moistened with 100-300 ml of fresh (unsalted) water for better contact. The IP receiver measures contact resistivity of each potential electrode; if the value is too high, you add more water to the electrode pit or look for a better grounding point within a 1-2 meter radius from the pegged point.

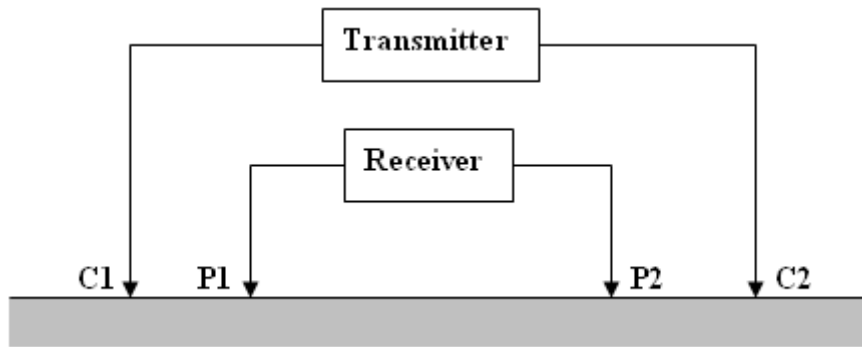


Figure 4-5: Typical four electrode array.

IP surveys are carried out along measurement lines, with readings taken on all measurement points, usually marked by the pegs labelled <Line>/<Point>. For example, a peg label that reads “1100/925” marks measurement point 925 on line 1100. Readings are taken from several potential dipoles (up to 8 with the IPR-12) simultaneously while the P electrodes are connected to the IP receiver using a multi-electrode potential cable or the “snake” (*a bunch of wires bundled together by insulation tape, with female connectors exposed where the electrodes are supposed to be connected to the “snake”*) enabling simultaneous measurements, and increased productivities.

The distance between the connectors corresponds to the distance between the measurement points. Therefore, if the point-to-point distance in the survey is 50 m, and using 6 potential dipoles (7 electrodes) for simultaneous readings, the “snake” will be 300 m long, with connectors exposed every 50 m.

Anomalously high values of chargeability typically correspond to the areas (zones) enriched with disseminated sulfides, which are the primary exploration target. Anomalously high values of apparent resistivity are often associated with quartz veins or BIF layers. A typical IP “signature” of a sulfide-bearing quartz vein is, therefore, a superposition of high apparent resistivity and high chargeability.

IP survey of a site is usually started in the profiling mode to delineate anomalous zones on the ground surface; the survey is continued in the sounding mode to trace the delineated anomalies to depth.

4.3. Quality control (QC)

The IPR-12 receiver has its own QC parameters, which are employed to ensure that the produced IP / resistivity data are of acceptable quality. They include the following:

SD (standard deviation) which defines data quality of the Mx measurements and in this case should not exceed 1.

RMS (root mean square deviation) quantifies the 'goodness' of the fit between the measured decay curve and the 'best fit' master curve. Any data with a RMS of greater than 3 was discarded and re-measured.

Copper sulfate electrodes always had a constant saturated solution (there should always be CuSO_4 crystals at the bottom) as potentials would be generated if any part of the solution was less than saturated.

Ensuring good insulation of all cables to avoid electrical leakages with a resultant noisy data.

During data acquisition, the following parameters were checked and always maintained above the required threshold. Where necessary, measurements were repeated: Primary voltage (V_p) had a minimum threshold of 20 mv, presence of spikes, decay curves shape and adequacy of the array.

4.4. Data transfer, processing and interpretation.

The acquired data are download from the IPR-12 receiver to a computer at the end of each field day, preferably immediately.

The IP data are processed with the use of the software package called Oasis montaj (by Geosoft). Gradient data are presented in form of maps while pole-dipole data are presented as pseudo sections. The data are further processed using inversions with RES2DINV or DCIP2D before interpretation is done.

5. CHAPTER FIVE: DATA ACQUISITION.

5.1. Survey grid

During the period from 2nd February to 14th April, 2012, both gradient and pole-dipole induced polarization and resistivity surveys were carried out on approximately 42 line kilometer grid known as Kamwango grid. The grid covered a 4 km² area that lies between latitudes 9922000mN and 9924000mN and longitude 677000mE and 679000mE. The survey was carried along lines running N-S (figure 5-1) in the study area. Gradient data were acquired on a line spacing of 100m and a point spacing of 25m. The survey lines were labeled as L100E to L2000E.

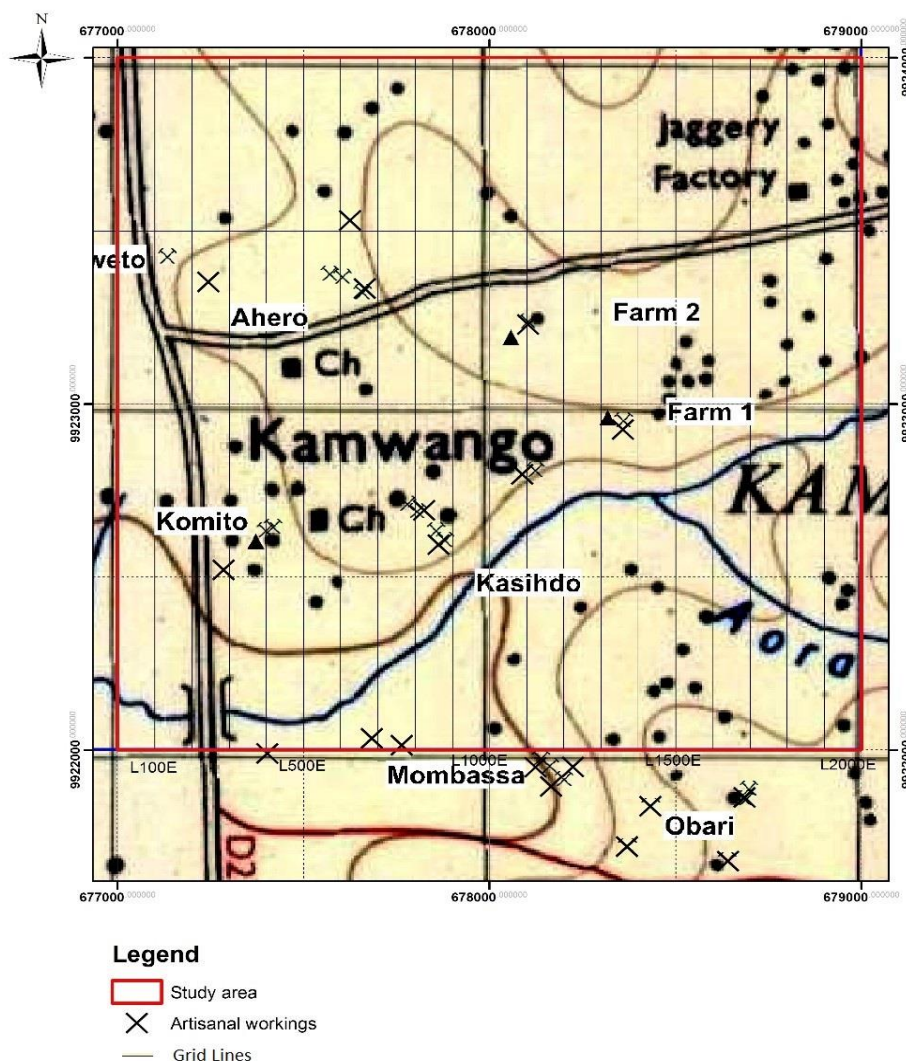


Figure 5-1: Kamwango grid (source: Kisii Topo Sheet).

The figure shows gradient survey lines (the black lines running N-S). Also shown in the figure are the numerous artisanal workings.

5.2. Field procedures.

There were three teams in the field:

The measurement team; this team consisted of one geophysicist and six local casual labourers, responsible for measurement of IP responses using the IPR-12 receiver.

The transmission team; the team consisted of one technician, one driver and two local casual labourers and was responsible for current transmission through the current lines.

The current line team; this team consisted of six casual labourers and a driver, they were responsible for laying the current lines. This included pulling the wire between the designated grounding locations, hammering in the electrodes, watering and salting the electrodes and connecting the electrode array to the wire.

5.3. Typical daily Schedule

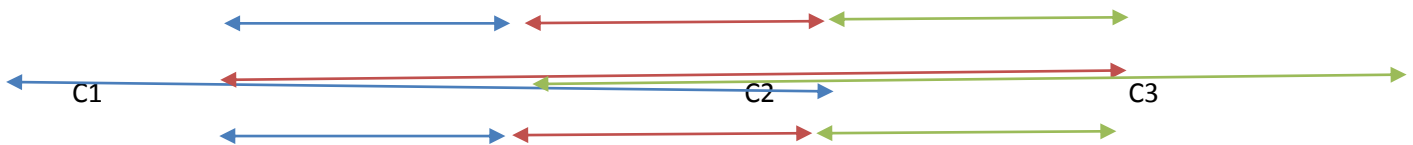
A typical day begins between 7:00 a.m. and 7:30 a.m. when the crew arrived on site, briefed on the day's work, safety and environment issues. The crew is then divided into the respective teams, as described in section 5.2, then dispersed to their respective stations to embark on their respective tasks.

From 7:30 a.m. to around 9:00 pm, the measurement team proceeds on foot to the first measurement location and sets up the measurement equipment. At the same time, the transmission team sets up at the first transmission location, ideally, a central location where current lines 1 and 2 can connect to transmission with ease, (figure 5-2). The team sets up the transmission equipment and communicate to all teams and stands-by for communication from the other teams. At the same time, the current line team moves to the first station and starts laying current line 1. When this is done, line attendants walk along the line making sure everything is set, then communication to confirm readiness is made to the rest of the teams.

From 9:00 a.m., when all teams are ready and have confirmed by radio, transmission of current begins. The technician in charge of transmission reads out the amount of current being transmitted from the transmitter and informs the geophysicist in charge of measurements. The team then measures up to 3 lines served by current line 1

(figure 5-2). During measurement, some of the current team members lay current line 2, connect it to the electrodes and go back to line 1. When measurement is done, the geophysicist informs the technician to switch off transmission and the teams to proceed to the next measurement locations; this process takes about one hour. The transmission team disconnects current line 1 and connects line 2, while the measurement team moves to the first measurement point of current line 2.

These procedures are repeated until the day ends at around 16:00 p.m. when the day's production targets have been met and the geophysicist in charge instructs all teams to pack up the equipment into the field vehicle. The crew meets, sets out the next day's work and leaves for camp.



where C : Current line

Figure 5-2: Illustration of current line arrangement

5.4. IP/Resistivity gradient

The survey lines are designed to cut across the local strike, measurements were performed with a view to showing reasonably clear zones of high apparent resistivity and high chargeability.

Gradient or modified Schlumberger array (figure 5-3) was used to acquire profile data. The array enabled acquisition of IP readings at multiple points with a single current line setup. Under rough field conditions, it also enabled working with reasonable productivity (Legault et al, 2015). For this array, the median depth of investigation (Z_e) is controlled by the current electrode separation ($L=C1C2$) according to $Z_e=0.191L$ (Edwards, 1977). Therefore, considering that, for this survey, $L= 900m$, the depth of investigation (Z_e) was 171.9m.

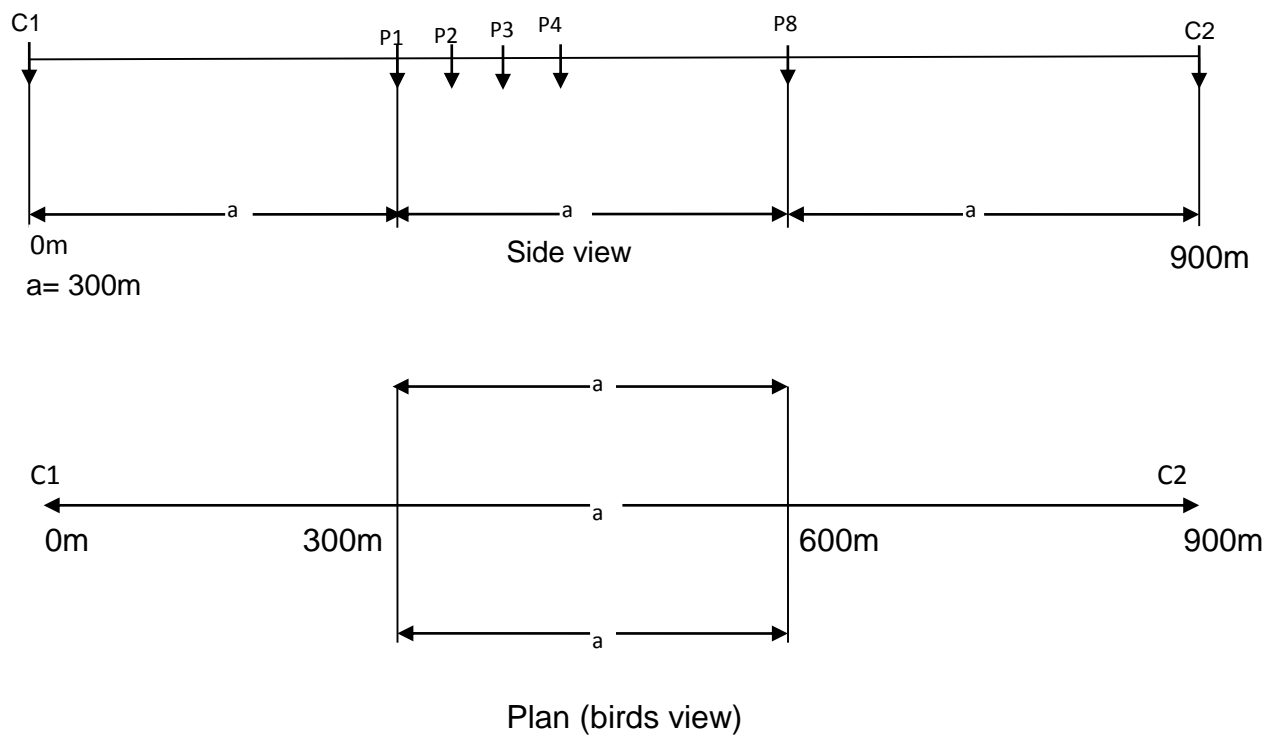


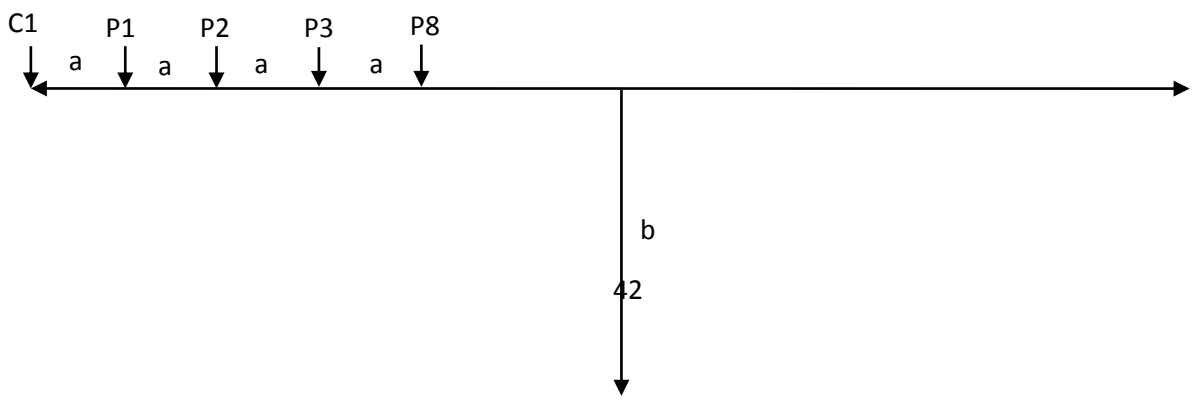
Figure 5-3: Side and plan view of the Gradient array (Source; AMS IP Manual).

The current dipole C1 C2 was 900 m long. The potential electrodes were placed at the middle third of the current dipole. For instance, in figure 5-3, when the first current electrode was placed at 0m the second was placed at 900m. The potential electrodes were placed from 300m to 600m. This arrangement allowed the measurement of two other lines adjacent to the central line without changing its location.

Potential electrode separation was fixed at 25m for the entire survey and data taken every 25m along the line. This survey arrangement provides a good combination of spatial resolution and sufficient signal strength for reliable measurements.

5.5. IP/Resistivity Pole-dipole

Soundings were performed over the chargeability and resistivity anomalies revealed by the IP gradient in order to trace the anomaly-generating bodies/zones to depth. Pole-dipole array (figure 5-4) was used to acquire the sounding data



a=25m

b=1200m

Figure 5-4: Illustration of pole dipole array (Source; AMS IP Manual)

The 'infinity' electrode, C2 was placed about 1.2km away from the measurement line at a right angle to the potential line, usually 8 times the size of the potential electrode cables.

The moving electrode C1 was always positioned 25 m away from the first potential electrode, for instance, from figure 5.4, when C1 was at 0m, the potential electrodes were placed at 25m, 50m, 75m, 100m..... until the final measurement station. The 25m separation was maintained throughout the measurement line. The procedure continued throughout the entire length of the line until P1 was at the last station and C1 was 25m away. Seven electrodes of six dipoles were used in this survey. For this array, the median depth of investigation (Z_e) is controlled by the current electrode separation ($a=P1P2$) according to $Z_e=2.478a$ (Edwards, 1977). Therefore, considering that, for this survey, $a= 25m$, the depth of investigation (Z_e) was 61.95m.

The IPR12 automatically recorded the following information with each reading: station location, 8 primary voltages in millivolts, 8 spontaneous potentials (sp) in millivolts, 8 secondary voltages (i.e. chargeability) in milliseconds (msec), transmitter current in milliamps, the number of stacks and finally time of the reading.

The data were stored with an associated header file which contained the common information for a collection of readings along a specific survey line. The position of all electrodes for any given dipole at any reading location can be derived from this header information.

The data were then downloaded from the IPR-12 receiver into a computer and stored as a dump file (in text format) for processing.

6. CHAPTER SIX: DATA PROCESSING.

6.1. Data processing.

The first data processing procedure was to edit the data and the header files in text format (figure 6-1) . The purpose of the procedure was to check and correct any mistakes from the manual numeric entries in the field, (for example, incorrect station number, incorrect dipole spread orientation, incorrect current, etc).

€

```

-----          S C I N T R E X          -----
-----

                IPR-12 MULTI-CHANNEL IP-RECEIVER V4.0

Job #:           25                        Date:         12/08/15
Operator:        JK                        Serial #:      1

P-Line:         1100E                      Units:
Metre

Array:  Pole-Dipole                        Mx From:     960 ms
To:  1050  ms

-----
-----

Station      P1      P2      P3      P4      P5      P6      P7
P8      P9

          C-Line      C1      C2      Curr.  Timing      Time  |
D:        VP      SP      Mx      S.D.      Res.      Dur.  K-
Fact.     Rho

          M1      M2      M3      M4      M5      M6      M7 |
M"      Tau

          M8      M9      M10     M11     M12     M13     M14 |
RMS%     Wi

*

    725N    725N    750N    775N    800N    825N    850N    875N
0+      0+

          1100E    700N    2000S    1200      2      14:13:23 |

```


1:	418.12	5	1.77	0.06	0.5		11	
314.2	109							
				7.27	6.27	5.47	4.69	35.4
0.12500								
	4.00	3.35	2.79	2.29	1.87	1.51	1.21	
0.544	11							
2:	144.22	10	1.78	0.05	0.2		11	
942.9	113							
				7.62	6.47	5.61	4.79	38.1
0.06250								
	4.08	3.39	2.80	2.30	1.88	1.50	1.21	
0.767	11							
3:	78.61	-11	1.94	0.13	0.6		11	
1886.8	124							
				8.05	6.90	6.01	5.13	40.8
0.06250								
	4.40	3.66	3.01	2.46	2.03	1.60	1.31	
0.917	11							
4:	67.06	1	1.98	0.15	0.7		11	
3146.6	176							
				8.23	7.05	6.15	5.24	41.7
0.06250								
	4.50	3.74	3.06	2.50	2.07	1.62	1.33	
1.029	11							
5:	61.63	2	1.80	0.54	0.9		11	
4723.4	243							
				7.41	6.36	5.56	4.77	36.0
0.12500								
	4.13	3.43	2.83	2.32	1.90	1.49	1.22	
0.959	7							
6:	61.31	10	1.81	0.67	0.7		11	
6618.5	338							

```

0.12500          7.38    6.33    5.53    4.73| 35.8
1.003    4.09    3.40    2.80    2.29    1.90    1.51    1.26|
           6

```

*

Figure 6-1: Pole Dipole data in text format.

The second process was to import the text file into Geosoft Oasis Montaj software. The software is able to import instrument dump files directly into an Oasis Montaj database. The database was saved and necessary corrections made using the quality control tool which enables one to delete any questionable noisy data. This procedure is subjective and is based primarily on the form of the secondary voltage decay, for example negative secondary voltages and secondary voltages with irregular, non-uniform decay curves were deleted and the data re-acquired. When the same problem re-occurred, the data were replaced with astericks.

The final data processing procedure was gridding and plotting the data into profile maps for gradient data (figures 6-1 and 6-2) and pseudosections for pole-dipole data (figures 6-3 to 6-9). Griding was done using bi-directional interpolation at a grid cell size of 100m, this gridding approach is used for ground data that has been collected along mostly parallel lines and interpolates the data at an equal interval along and across the survey lines.

6.2. Results.

6.2.1. Gradient maps.

Gradient data were plotted into color coded contour maps. The maps show zones of high and low apparent chargeability and resistivity (figures 6-1 and 6-2). The maps are color coded contour maps with a color scale on the side, where the pink zones indicate zones of high chargeability or resistivity and the blue zones indicating zones of low chargeability or resistivity. The data plots shown were directly interpretable in a qualitative manner as high chargeability may be related to conductive structures near the surface or at greater depth while high apparent resistivity is due to high resistive units at or near the surface. Due to the disseminated nature of the ore body, it is more likely to have high resistivity correlated to high chargeability. Therefore, zones with both high chargeability and high resistivity or high chargeability and high resistivity occurring close to each other were selected for follow-up using pole-dipole array to delineate these anomaly causing zones to depth.

From the Rho and Mx maps, seven lines were selected on the basis of; zones with both high mx and Rho or with these zones close to each other, anomalous soil sampling zones previously done by Stockport and artisanal workings. The lines are: L 500E (50S-1200N), L600E (50S-1275N), L900E (50S-2000N), L1000E (450-1500N), L1100E (700-2000N), L1900E (850-1500) and L2000E (925-1800N). The lines are shown on the gradient maps in orange (figure 6-1 and 6-2).

The raw Pole-dipole data were presented in form of pseudo-sections (figures 6-3 to 6-9) which are mathematical models calculated to match each readings theoretical position below the surface.

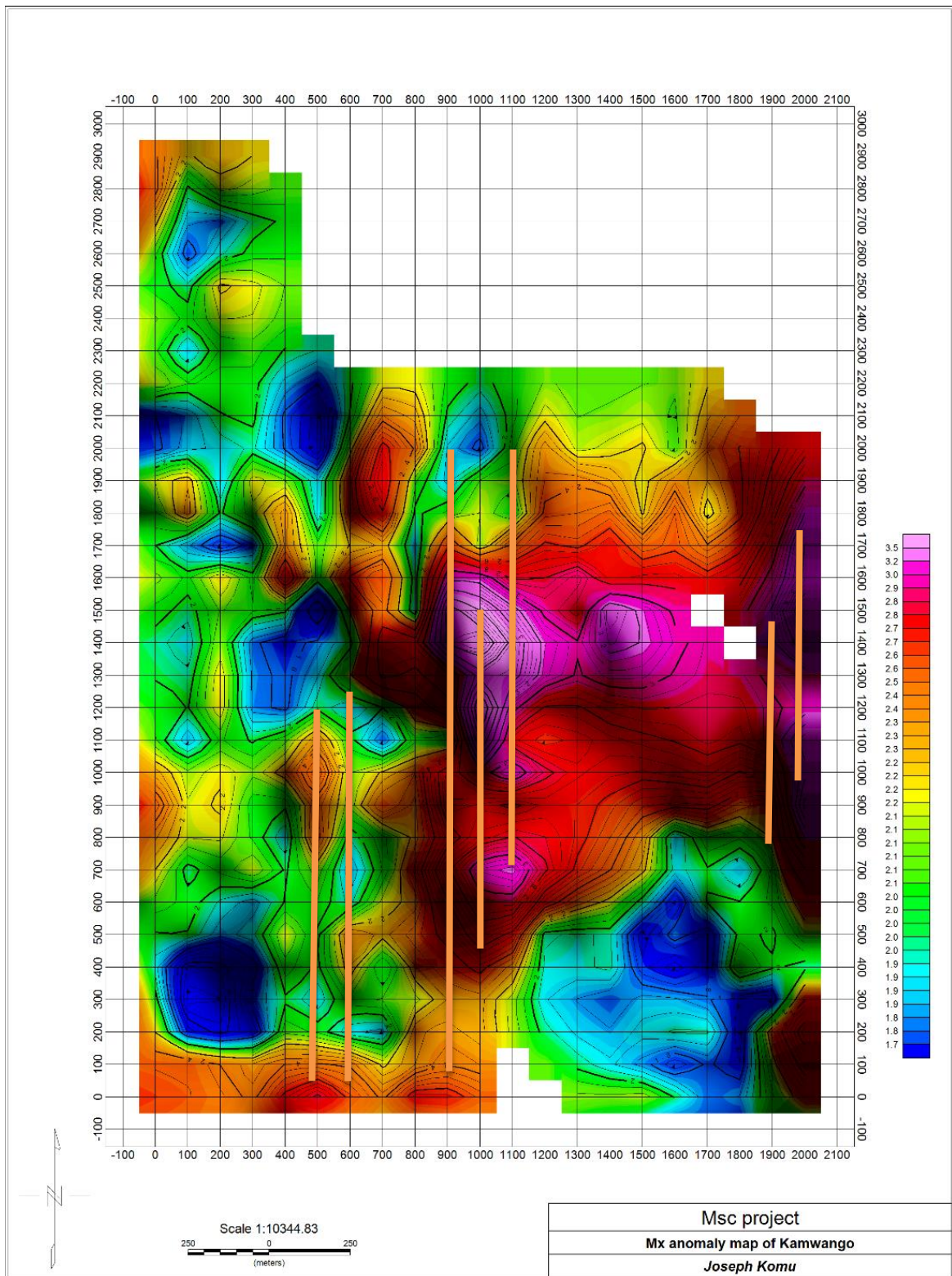


Figure 6-1: Chargeability anomaly map.

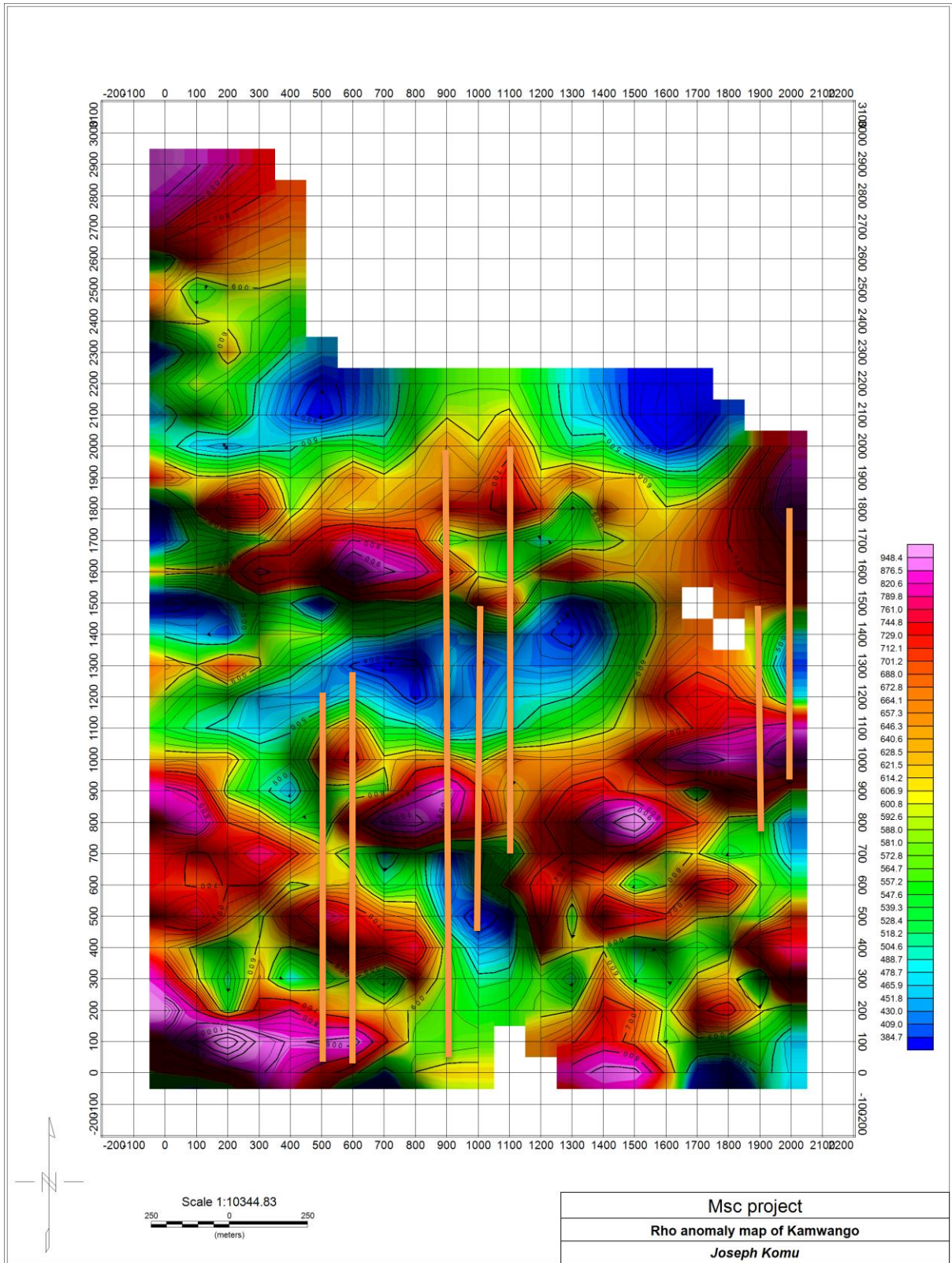
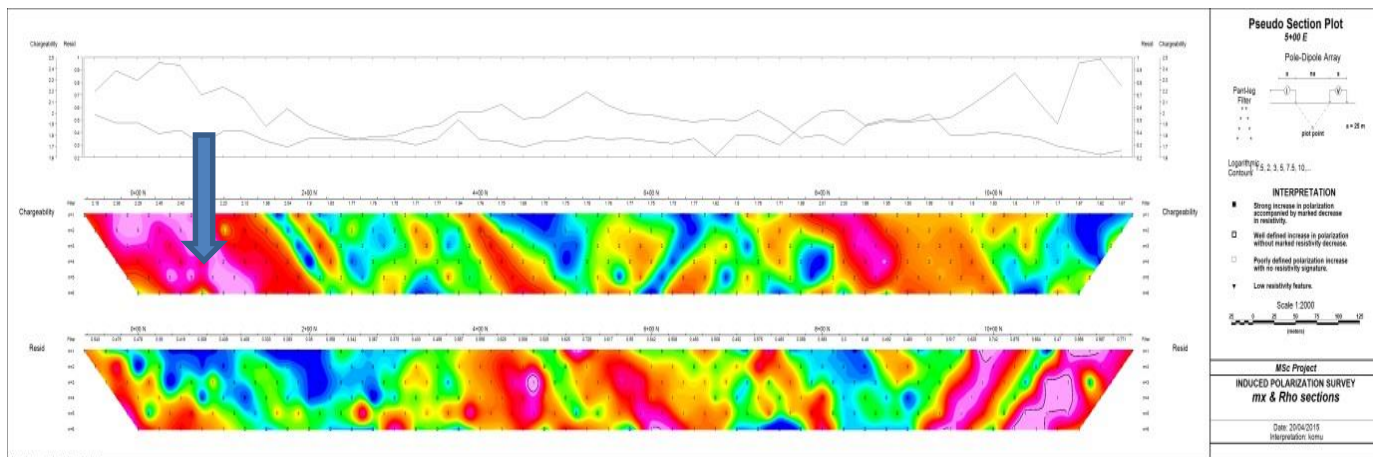


Figure 6-2: Resistivity anomaly map.

6.2.2. Pole Dipole Pseudo sections.

L 500E

Figure (6-3) represents color coded chargeability and Resistivity sections of L 500E. Pink color indicates high chargeability and high resistivity zones, while the blue color indicates low chargeability and resistivity zones. High chargeability indicates probable conductive zones while high resistivity indicate highly resistive units. The blue arrow points to a high chargeability zone which is a good target for follow up.

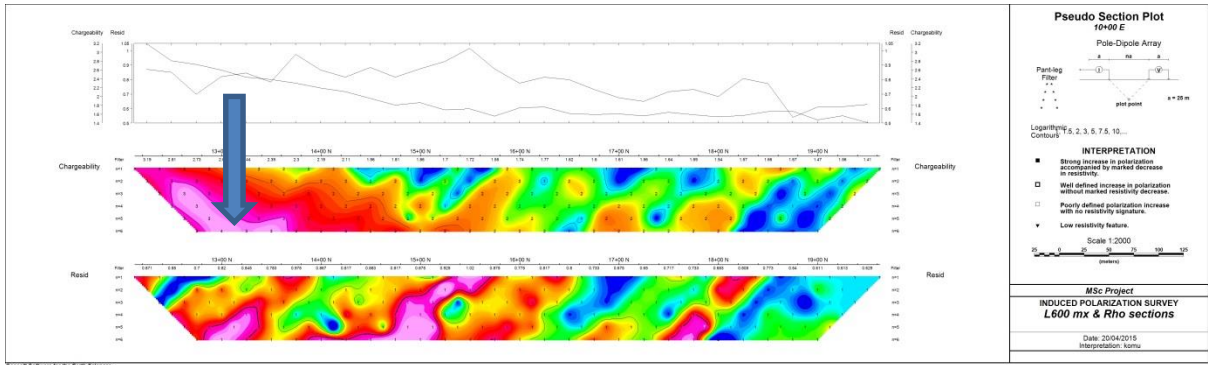


➡ IP Target

Figure 6-3: L 500E

L 600 E

Figure (6-4) represents color coded chargeability and Resistivity sections of L 600E. Pink color indicates high chargeability and high resistivity zones, while the blue color indicates low chargeability and resistivity zones. High chargeability indicates probable conductive zones while high resistivity indicate highly resistive units. The blue arrow points to a high chargeability zone which is a good target for follow up.

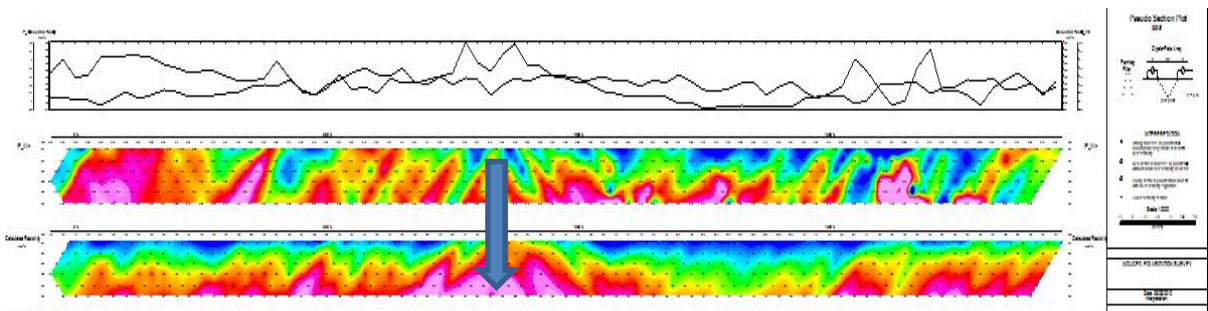


➔ IP Target

Figure 6-4: L 600E

L 900E

Figure (6-5) represents color coded chargeability and Resistivity sections of L 900E. Pink color indicates high chargeability and high resistivity zones, while the blue color indicates low chargeability and resistivity zones. High chargeability indicates probable conductive zones while high resistivity indicate highly resistive units. The blue arrow points to a high chargeability zone which is be a good IP target for follow up.



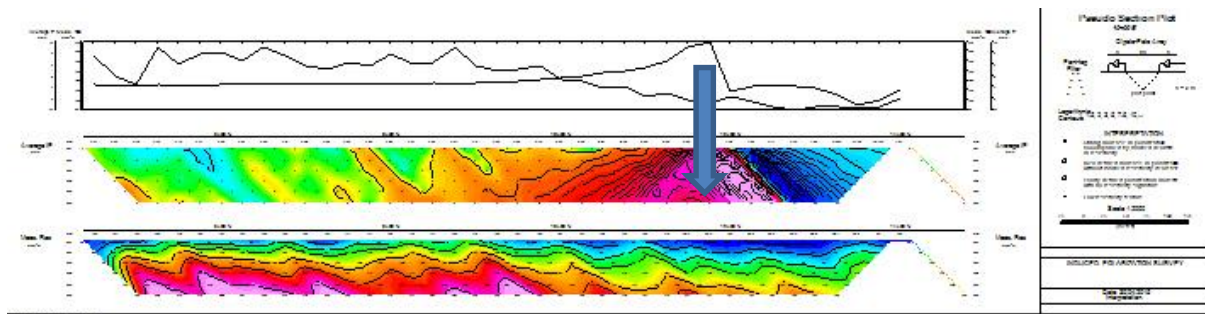
➔ IP Target

Figure 6-5: L 900E

L1000 E

Figure (6-6) represents color coded chargeability and Resistivity sections of L 1000E. Pink color indicates high chargeability and high resistivity zones, while the

blue color indicates low chargeability and resistivity zones. High chargeability indicates probable conductive zones while high resistivity indicate highly resistive units .The blue arrow points to a high chargeability zone which is a good target for follow up.

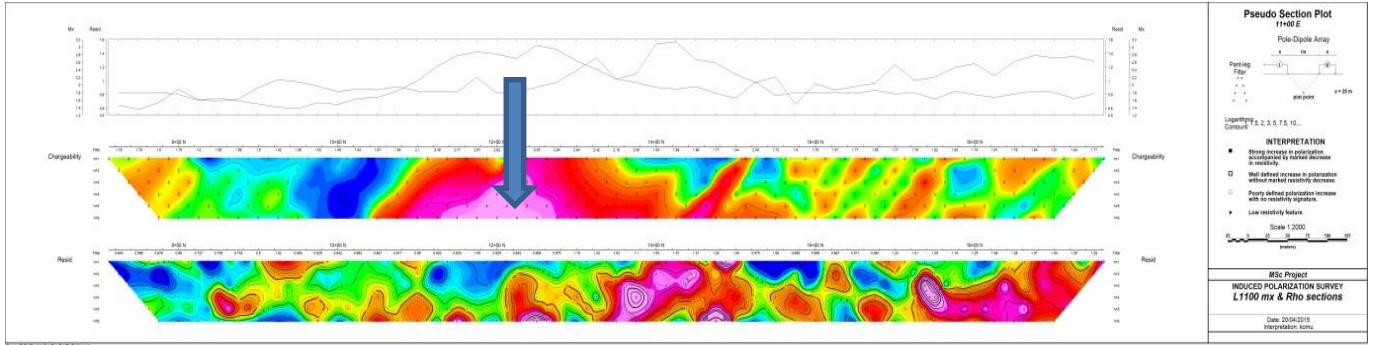


➔ IP Target

Figure 6-6: L1000E

L 1100E

Figure (6-7) represents color coded chargeability and Resistivity sections of L 1100E. Pink color indicates high chargeability and high resistivity zones, while the blue color indicates low chargeability and resistivity zones. High chargeability indicates probable conductive zones while high resistivity indicate highly resistive units .The blue arrow points to a high chargeability zone which is a good target for follow up.

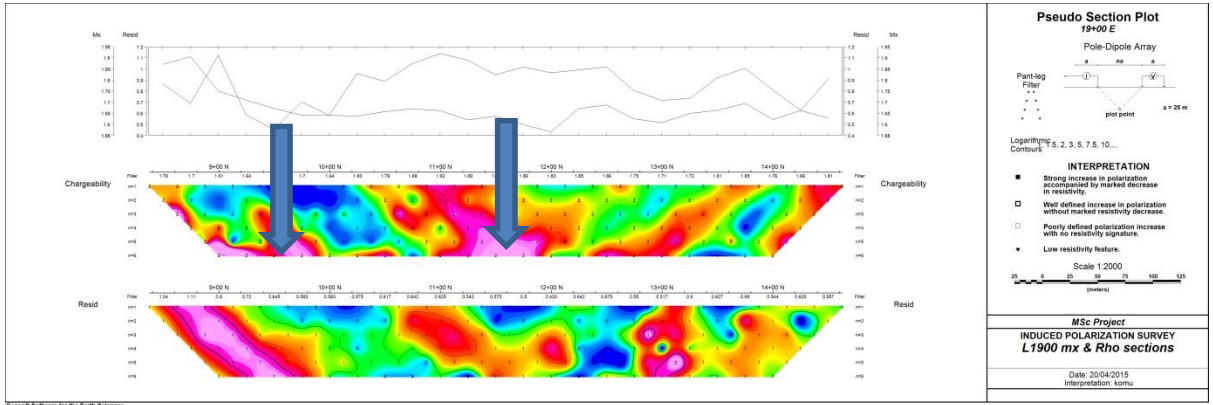


➔ IP Target

Figure 6-7: L1100E

L 1900E

Figure (6-8) represents color coded chargeability and Resistivity sections of L 1900E. Pink color indicates high chargeability and high resistivity zones, while the blue color indicates low chargeability and resistivity zones. High chargeability indicates probable conductive zones while high resistivity indicate highly resistive units. The blue arrows points to high chargeability zones which are good target for follow up.

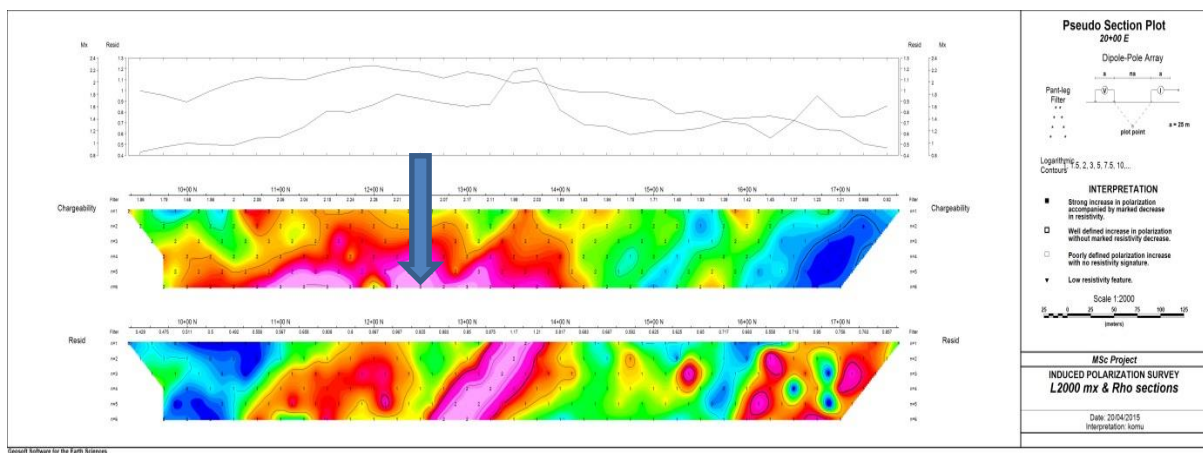


➔ IP Target

Figure 6-8: L1900E

L 2000E

Figure (6-9) represents color coded chargeability and Resistivity sections of L 2000E. Pink color indicates high chargeability and high resistivity zones, while the blue color indicates low chargeability and resistivity zones. High chargeability indicates probable conductive zones while high resistivity indicate highly resistive units. The blue arrow points to a high chargeability zone which is a good target for follow up.



➔ IP Target

Figure 6-9: L2000E

From the sections, anomaly causing units were traced to depth. These sections were interpretable qualitatively. Areas with high apparent Chargeability and Resistivity can be interpreted to be zones with probable highly conductive materials in this case sulfides and highly resistive materials such as silicates respectively.

The pseudo sections are deceptive and do not present the true distribution of material properties in the ground. To achieve the true distribution of properties, inversion was done using RES2DINV software. The resulting resistivity model reveal information about rocks overlying the deposit and structures, while the resulting chargeability model shows the deposit itself. See figures 6-10 to 6-16.

6.2.3. Inversion models and Interpretation.

There are generally two approaches to calculate IP effect from mathematical models Loke (2015), the complex resistivity method and the perturbation method. The later method, which was used in the in this research considers the IP model as a small perturbation of the base resistivity model.

Li and Oldenberg (1994) described the IP inversion as a two-step process. First, a resistivity inversion using only resistivity data is carried out. This produces a resistivity model (ρ_{DC}) that is independent of the measured data. Secondly, the apparent IP values are calculated using the resistivity model as a base and the equation m . While keeping the resistivity model fixed, the apparent IP data was then inverted to obtain a chargeability model (M_{IP}).

The results and interpretation of each line is given on figures 6-10 to 6-16. Generally, highly resistive units are observed on the south part of the models; they appear to extend considerably in depth and are likely geological units, in this case, highly resistive basement rocks. The anomalies broaden and appear stronger with depth. The top of the source is, in general, shallow lying at a depth of around 40m. Since some of the zones of high chargeability shown in the models correspond or are next to highly resistive zones, then, these zones exhibiting distinct anomalies can be mapped out as possible areas of disseminated sulfide mineralization, with increasing concentrations towards the center of the disseminated material.

L 500E: Mx and Rho inversions and Interpretation.

From figure 6-10, a prominent IP anomaly extending from 100mN to 250mN is observed at zone marked A. The dyke like anomaly is strong, dips S.E and seems to extend to the surface, though weak towards the surface; probably due to weathering of the sulphide body on the surface. Interesting features of high and low Rho (shown in black dotted lines) can be seen on the same zone A and also on zone C on the Rho model; this could be interpreted to be quartz veins.

A second IP anomaly can be seen right next to the vein like features on zone C, this is however not easily interpretable as it is not very clear and does not seem to extend to the surface.

There are active artisanal workings near both zone A and C (figure 6-17). These workings increases the confidence of the two target zones.

One drill holes were proposed at 250 mN and named BH 1, see figure 7-1. The bore hole is shown on zone A in the model is designed to be inclined at an angle of about 45°, such that it cuts the dyke like IP.

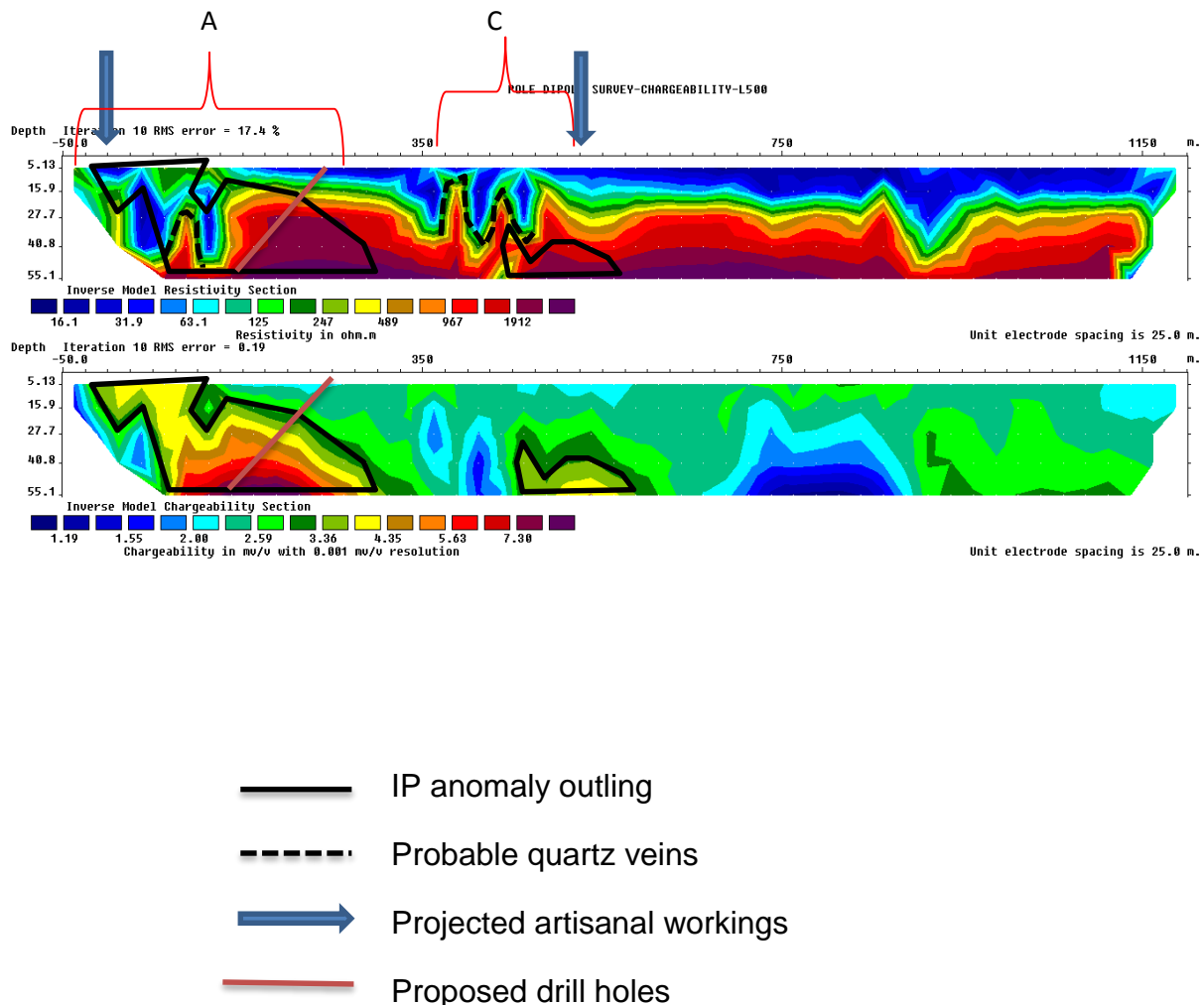


Figure 6-10: L 500E Mx and Rho inversions and Interpretation.

L 600: Mx and Rho inversions and Interpretation

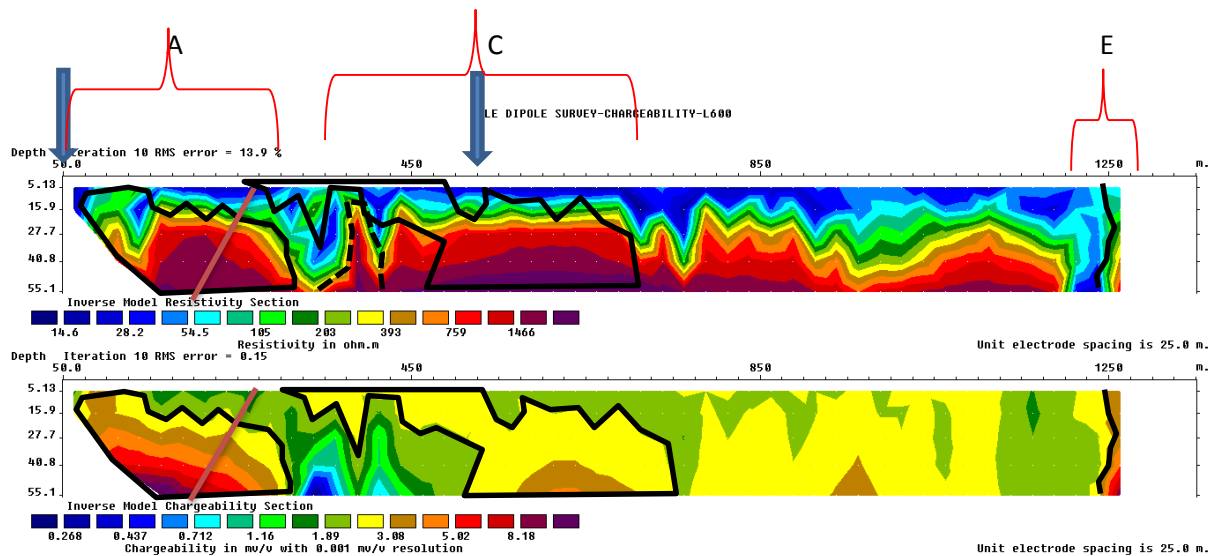
On figure 6-11, an IP anomaly can be observed at the SW corner of the plot on zone A. The anomaly is strong and seems to be the same zone extending from L500E (figure 6-17). It extends from around 50mN to 250mN and dips NW to SE, on the model.

A second IP anomaly can be seen on zone C which seems to be the same zone extending from L500 (figure 6-17), it looks weak but extends to the surface. The IP anomaly lies next to a prominent geological structure, probably quartz vein, shown by the black dotted line in the Rho model.

There are active artisanal workings near both targets as shown on the models (figure 6-17).

Another IP anomaly can be observed at zone E, It lies next to a prominent geological structure shown as the very low resistivity zone on the Rho model and also shown as a geological contact between the Kamwango shear zone and agglomerates (figure 6-18). The IP anomaly is very difficult to interpret as the model is not conclusive.

One bore hole was proposed from the models in zone A and named BH 2 at 275mN (figure 7-1). The bore hole was designed to cut the high IP anomaly at around 45°.



- IP anomaly outline
- - - - Probable quartz veins
- Projected Arisinal workings.
- Proposed drill holes

Figure 6-11: L 600E Mx and Rho inversions and Interpretation.

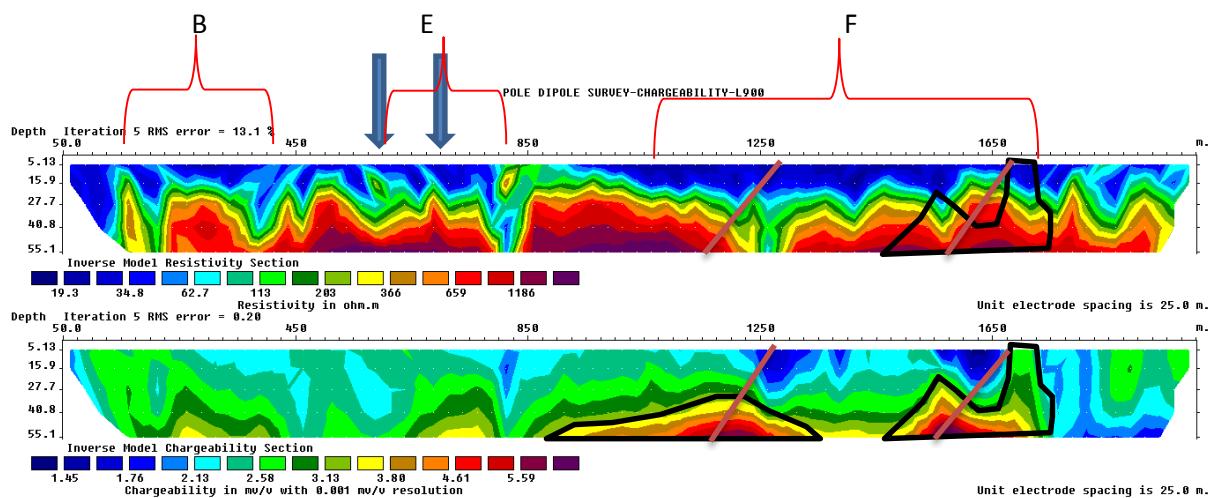
L 900: Mx and Rho inversions and Interpretation.

From figure 6-12, small IP anomalies can be seen in both zones B and E. There are also some quartz like structures highlighted by the dotted line in the Rho model. Zones B could be the same anomalous zones extending from Lines 500E and 600E on zone C (figure 6-17).

Two strong IP anomalies can be seen on zone F, one extending from 1050mN to 1300mN and the second extending from 1500mN to 1700mN. The prominent geological structure seen in the Rho model at around 850mN is most possibly the I contact zone between the Kamwango shear zone and the agglomerate (figure 6-18).

There are two active artisanal workings near target zone E (figure 6-17).

Two drill-hole were proposed from this model in zones F and named BH 3 at 1275 mN and BH 4 at 1675 mN (figure 7-1). The two were designed to be inclined at around 45°, to try intercept the IP anomaly.






-  IP anomaly outline
-  Projected Artisanal workings
-  Proposed drill holes

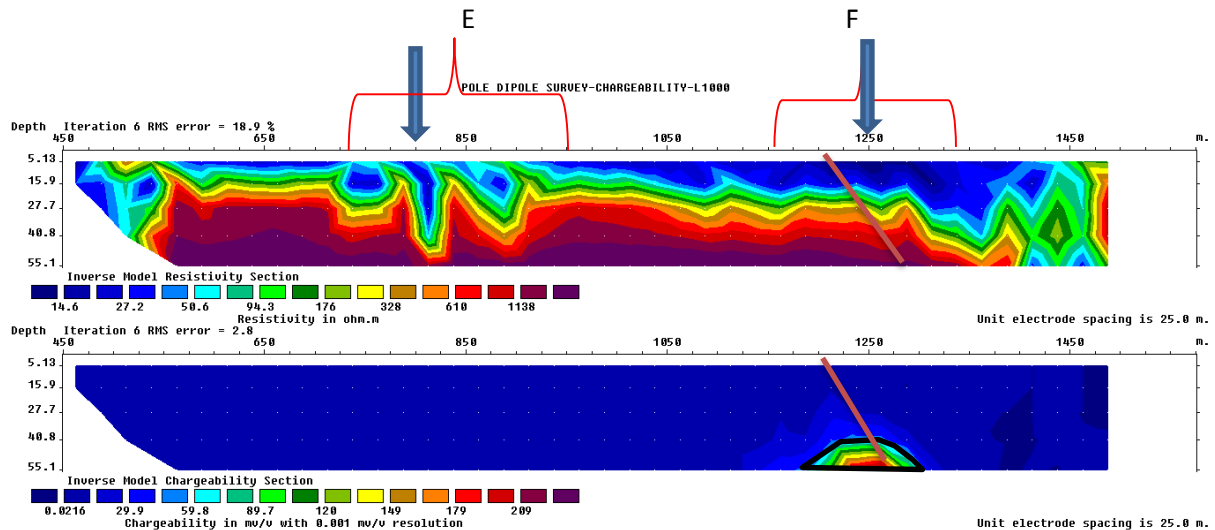
Figure 6-12: L 900E Mx and Rho inversions and Interpretation.

L 1000: Mx and Rho inversions and Interpretation.

From figure 6-13, a strong IP anomaly can be seen on zone F extending from 1200mN to 1300Mn, it seems to be the same zone extending from L900E (see figure 6-17). This is around the same area where previous drill holes were done shown on figures 2-4 .From the resistivity model, a prominent geological feature can be seen at

around 1450mN. This could possibly be the geological contact between the Agglomerate and the vesicular lava (figure 6-18). There are two artisanal workings one is near the vein like structures at around 850mN and the second at zone F.

One borehole was proposed from this model in zone F and was named BH 5 at 1200MN to test the IP anomaly (figure 7-1). The borehole was also designed to be inclined at around 45° so as to intercept the IP anomaly.



- Anomaly outline
- ➔ Projected Artisanal workings
- Proposed drill holes

Figure 6-13: L 1000 Mx and Rho inversions and Interpretation

L 1100: Mx and Rho inversions and Interpretation.

From figure 6-14, a strong IP anomaly can be seen on zone F extending from 1175mN to 1300mN. The zone seem to extend to the surface, though weak towards the surface, probably due to weathering towards the surface. This zone is around the same area where previous drill holes were done as shown on figure 2-4 and seems to be the same zone extending from L1000E and L900E (figure 6-17).

An artisanal pit sits right above this target zone as shown on figures 6-14 and 6-17.

One bore hole was proposed from the model in zone F and was named BH 6 at 1225mN (figure 7-1). It was designed to be inclined same as the IP anomaly.

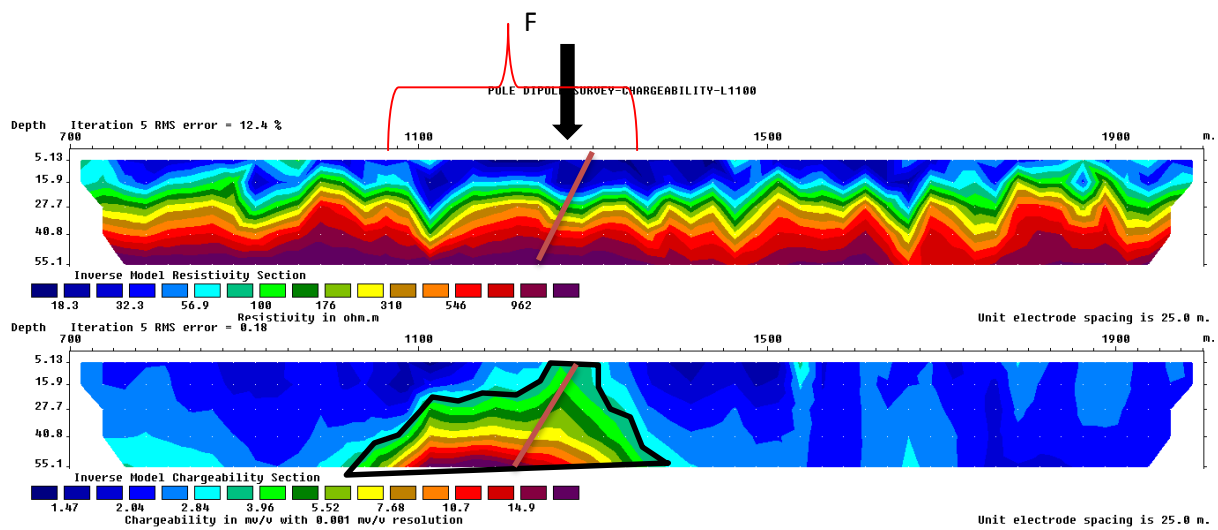


Figure 6-14: L 1100 Mx and Rho inversions and Interpretation

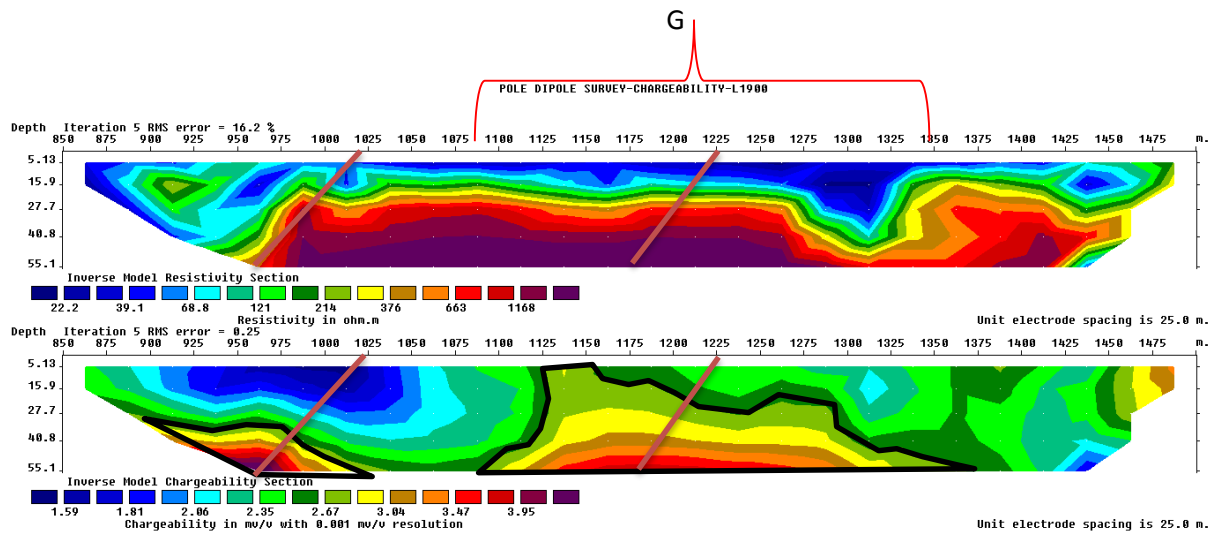
L 1900: Mx and Rho inversions and Interpretation.

From figure 6-15, the first IP anomaly is seen in the right corner of the plot extending from 925mN to 972mN. This is quite difficult to interpret as the zone is not complete on the model.

A second prominent IP anomaly can be seen on zone G extending from 1125mN to 1300mN. It seems to extend towards the surface though weak towards the surface.

It is difficult to tell whether the zone is an extension of zone F on any other zones to the west due the big distance between L 1100 and L 1900.

Two boreholes were proposed from this model in zone G one at 1025 mN and the second at 1225 mN .The boreholes were named BH 7 and BH 8 respectively and were designed to cut the IP anomalies at 45° .



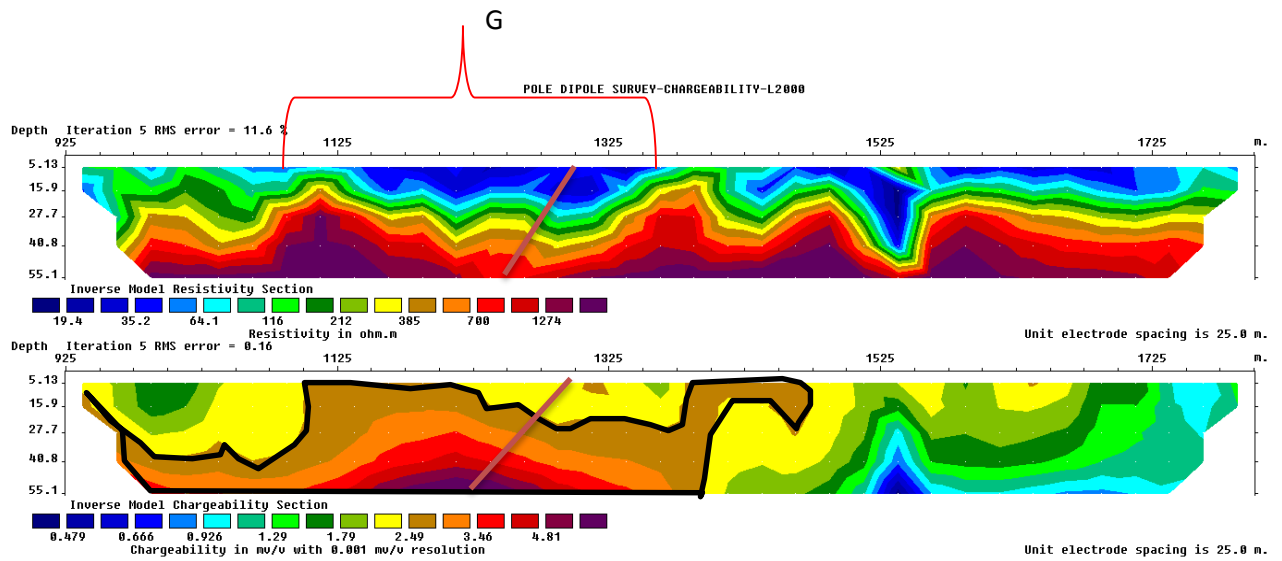
- Anomaly outline
- Proposed drill hole

Figure 6-15: L 1900 Mx and Rho inversions and Interpretation

L 2000: Mx and Rho inversions and Interpretation.

From figure 6-16, a strong IP anomaly can be seen zone G, it extend from 1100mN to 1325mN and seems to extend towards the surface. It seems to be the same zone extending from L1900E (figure 6-17).

One borehole was proposed from this model in zone G named BH 9 at 1300mN and (figure 7-1). The borehole was designed to be inclined at around 45⁰.



- Anomaly outline
- Proposed drill holes

Figure 6-16: L 2000 Mx and Rho inversions and Interpretation.

A plan view map of the Models interpretation showing PDP lines in black lines, areas of IP anomaly in green and probable quartz veins in red; artisanal mines in an x and possible mineralized zones A, B, C, D, E, F and G is shown on figure 6-17. A plan view map of the results superimposed on the geological map is shown on figure 6-18.

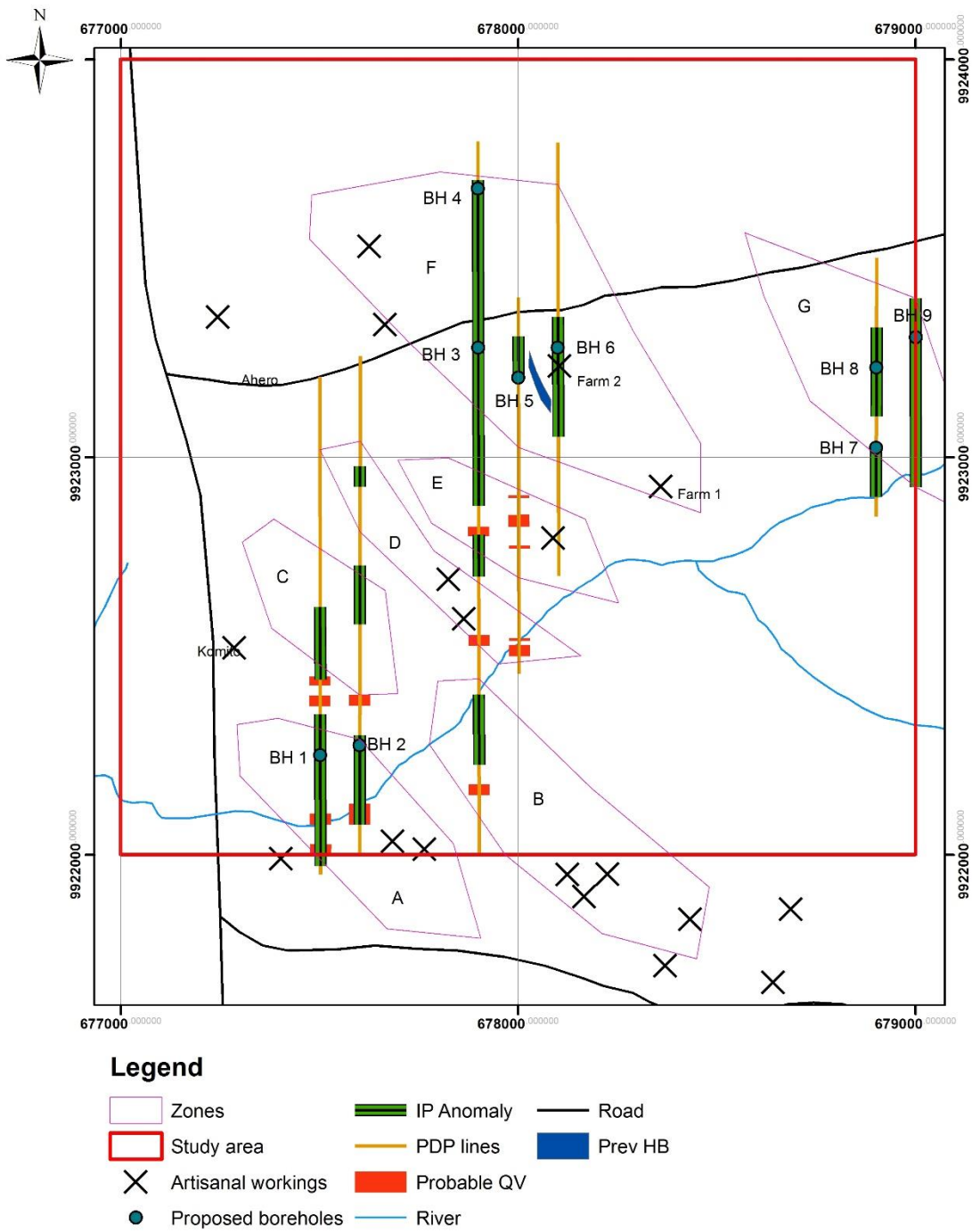


Figure 6-17: Plan view map of the Model interpretations.

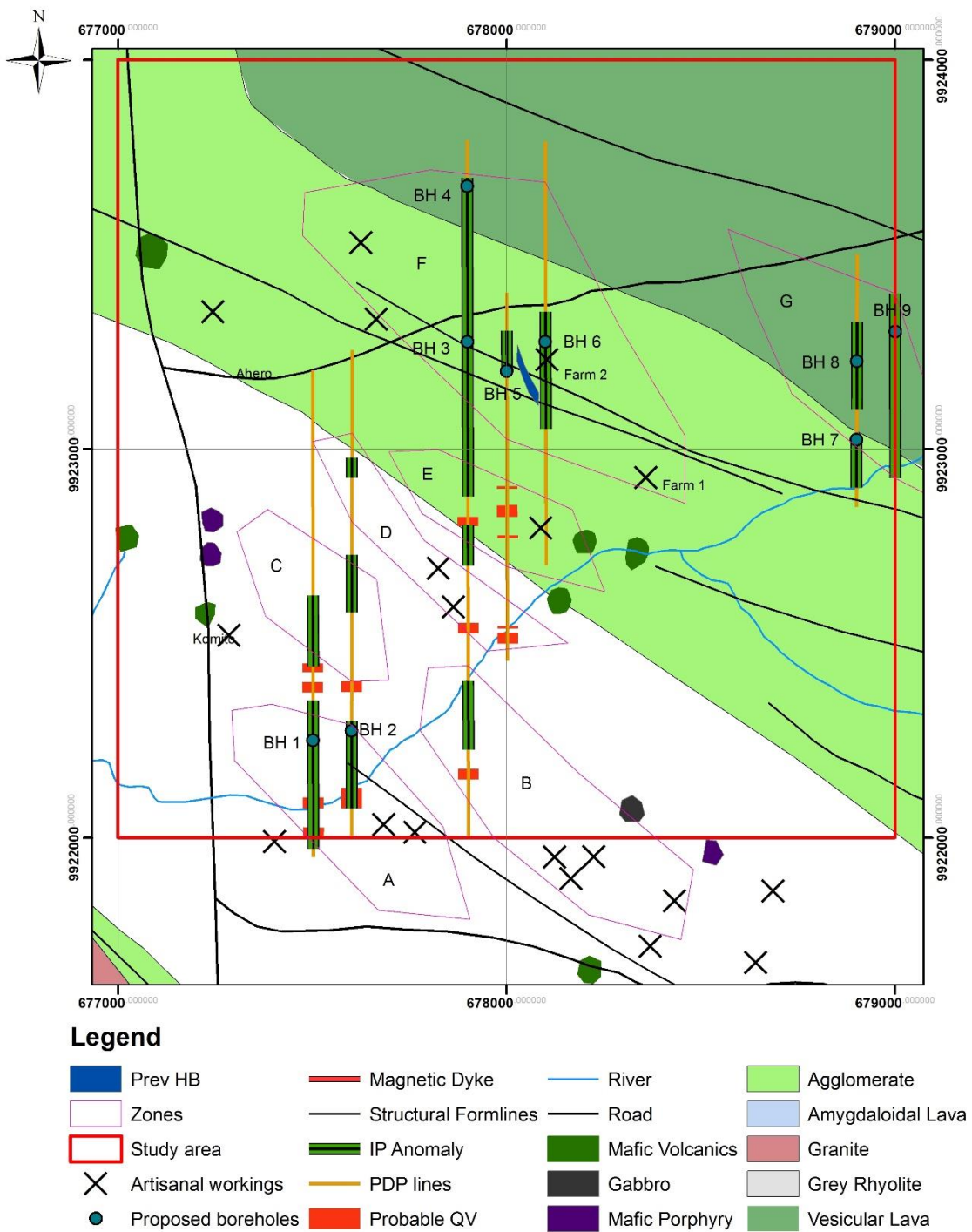


Figure 6-18: figure 6-17 superimposed on the geological map

7. CHAPTER SEVEN: DISCUSSION, CONCLUSION AND RECOMMENDATIONS

7.1. Discussion

Several prominent possible mineralization zones were identified from the study area, the zones are quite extensive, trend NW-SE and continuous as they extend from one survey line to the next (figure 6-17). The NW- SE trend is consistent with the general trend of geological formations and structural formlines (figure 2-2 and 2-3). The zones are most prominent in the Kamwango shear zone and the agglomerates with zones D and E occurring near the contact between the agglomerate and the Kamwango shear zone and zone G and F near the agglomerates and vesicular lava contact (figure 6-18).

The viability of these zones can be supported by the numerous artisanal workings around them, as shown on the models from figures 6-10 to 6-16 and figures 6-17 and 6-18

Areas on the possible mineralized zones that revealed high IP (possible sulphides) and High Rho features (Possible quartz veins) superimposed or next to each other were selected for follow-up drilling as they reflect the main type of mineralization of the study area, (near surface stockworks of gold-bearing quartz veins and sheet swarms with the gold being associated with sulphides such as galena and pyrite) as indicated in section 2.6.2. The proposed boreholes as marked on the inversion models, are designed to dip at around 45° . This way, the boreholes cut across the targeted zones and increase the probability of hitting good targets during drilling.

Previously drilled test holes shown on figure 2-4 occurs on zone F where BH 5 and BH 6 have been proposed. Results from the previous boreholes have given grades of up to 81.4 g/t Au (figure 2-4). This shows that the geophysical method is a useful method in surveying for mineralized zones for drilling.

Some of the challenges faced included;

- Noise from power lines and pirate electricity connection in the study area.

The study area has power lines, which is a major source of noise in IP surveys. Moreover, locals in the area have pirated electricity from the power lines to their homes. This made an already bad situation worse. During the survey, power had to be switched off in the area to enable acquisition of clean data, this caused delays and in some areas data was not acquired at all.

This challenge could turn out to be a good geophysical project whereby one could study the impact of noise from power lines on IP data.

- Access to processing and inversion software.

Geophysical data processing softwares are very expensive. Moreover, getting a software that does exactly what one wants is next to impossible. One is forced to use several software to complete the whole process. I had access to an Oasis Montaj license. However, this software does not do inversions of IP and Resistivity data. I later used RES2DINV to do the inversions thanks to my supervisor Prof Barongo.

7.2. Conclusion

The aim of this research was to use induced polarization and Resistivity methods in the search for possible gold mineralization in the study area. 42 line kilometer of gradient IP and Resistivity was done in the area to try and reveal IP and Resistivity anomaly zones in the gradient mode, later, anomalous zones revealed from the gradient maps were followed up with pole dipole method to trace the anomaly causing zones to depth. This data was inverted and interpreted and most potential targets recommended for follow up drilling.

Six possible mineralized zones were revealed from the interpretations (figure 6-17). The fact that one of the zones occurs on the area where previous boreholes were done by the license holder shows that the method was a success and quite useful in the survey of this type of gold mineralization. A total of nine boreholes were proposed for follow-up drilling from the interpreted models (figure 7-1). The recommended boreholes coordinates are listed below.

BH 1: 677500mE, 9922250mN

BH 2: 677600mE, 9922275mN

BH 3: 677900mE, 9923275mN

BH 4: 677900mE, 9923675mN

BH 5: 678000mE, 9923200mN

BH 6: 678100mE, 9923225mN

BH 7: 678900mE, 9923025mN

BH 8: 678900mE, 9923225mN

BH 9: 679000mE, 9923300mN

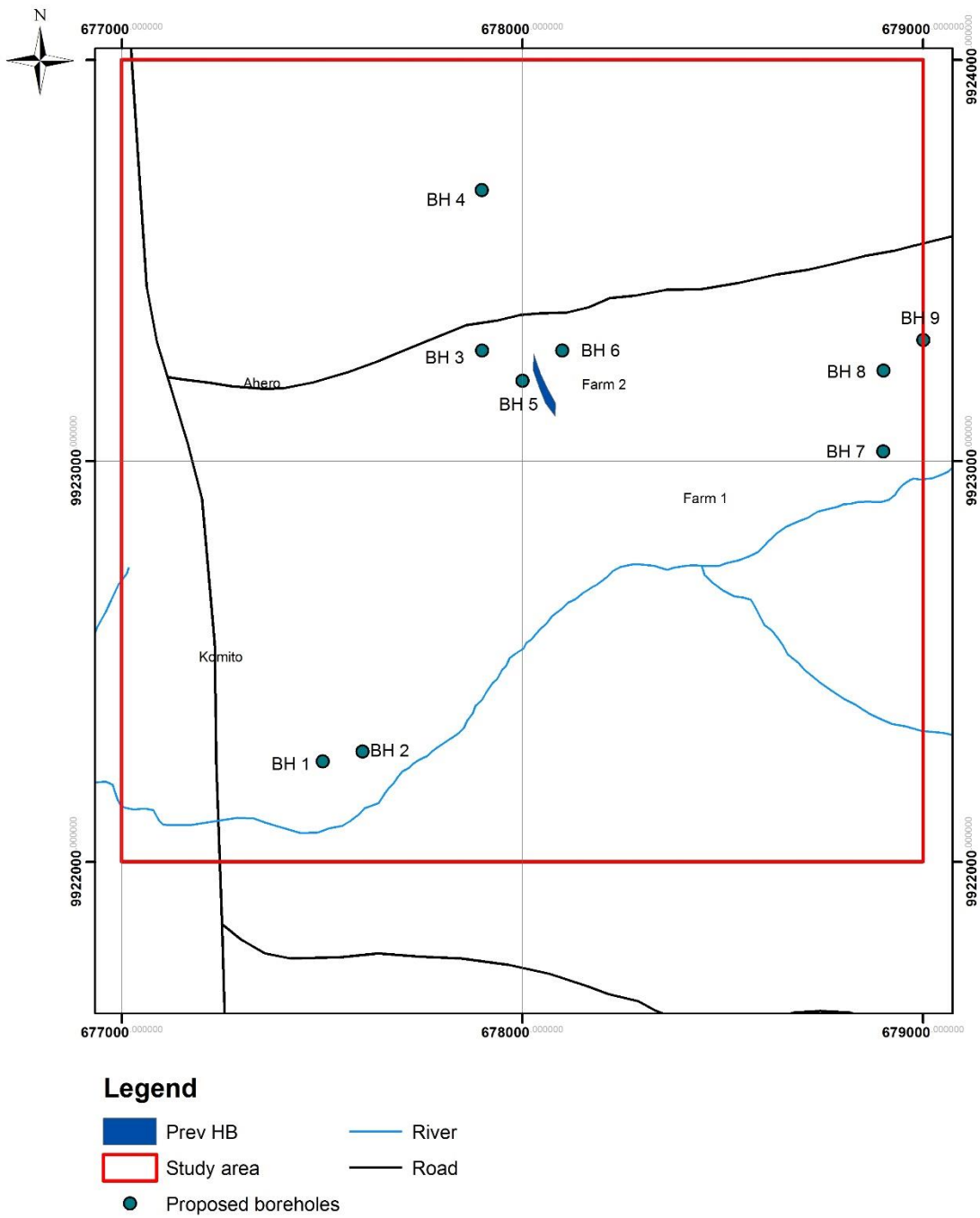


Figure 7-1: Location of nine proposed boreholes.

7.3. Recommendations.

1. Boreholes 1 to 9 in zones A, B, C, E, F and G were seen to be the most viable and are recommended for follow-up drilling as they give the best indication for gold mineralization.
2. If resources are available, boreholes can be done on zone C on L 500E and L 600E next to the quartz vein structures.
3. One or two PDP line be surveyed between L1100E and L1900E, this will help check whether zone F extend to zone G and get more drill targets around farm 1 artisanal mine.

8. REFERENCES

African queen mines signs earn-in and JV agreement for Rongo gold field project in Kenya's Lake Victoria Greenstone Belt, May 17 2010 Issue.

Aiken, C. L., Hastings, D. A., & Sturgul, J. R. (1973). Physical and Computer Modeling of Induced Polarization*. *Geophysical Prospecting*, 21(4), 763-782.

Bertin, J. and Loeb, J. (1976). Experimental and Theoretical Aspects of Induced Polarisation, volume 1 of 1. Gebrüder Borntraeger, Berlin.

Butler, D. K. (Ed.). (2005). *Near-surface geophysics*. Tulsa: Society of Exploration Geophysicists.

Butler, D. K., Zonge, K., Wynn, J., & Urquhart, S. (2005). 9. Resistivity, Induced Polarization, and Complex Resistivity. In *Near-surface geophysics* (pp. 265-300). Society of Exploration Geophysicists.

Dobrin, M. B., & Savit, C. H. (1960). Introduction to geophysical prospecting. McGraw-Hill Book Company.

Grantham, D. R., McConnell, R. B., & Temperley, B. N. (1945). *Explanation of the geology of degree sheet no. 17 (Kahama)*. Government Printer, South Africa.

Gómez-Ortiz, D., Martín-Velázquez, S., Martín-Crespo, T., Márquez, A., Lillo, J., López, I., ... & De Pablo, M. A. (2007). Joint application of ground penetrating radar and electrical resistivity imaging to investigate volcanic materials and structures in Tenerife (Canary Islands, Spain). *Journal of applied geophysics*, 62(3), 287-300.

Hitchen, C. S. (1937). Geological survey of Kenya of no. 2 mining area, Kavirondo.

Huddleston, A. (1951). *Geology of the Kisii district*. Geological Survey of Kenya.

Ichang'i, D. W. (1993). Segment of the Nyanza Greenstone Belt, Kenya. In *Proceedings of the Fifth Conference on the Geology of Kenya on Geology for Sustainable Development* (p. 78). Geological Society of Kenya.

Keller, G. V. and Frischknecht, F. C. (1966). Electrical Methods in Geophysical Prospecting, volume 10. Pergamon Press Inc.

Legault, J. M., Niemi, J., Brett, J. S., Zhao, S., Han, Z., & Plastow, G. C. (2016). Passive airborne EM and ground IP resistivity results over the Romero intermediate sulphidation epithermal gold deposits, Dominican Republic. *Exploration Geophysics*.

Li, Y. and Oldenburg, D.W., 1994, Inversion of 3-D dc resistivity data using an approximate inverse mapping: *Geophysical Journal International*, 109, 343-362.

Loke M.H., and Barker, R., 1996, Rapid least-squares inversion of apparent resistivity pseudosections by a quasi-Newton method: *Geophysical Prospecting*, 44, 131-152.

Loke, M. H. Baker, R. D., 1995, least square decomposition of apparent resistivity pseudosections", *Geophysics* vol. 60, No. 6, 1682-1690.

Loke, M. H., Wilkinson, P. B., Chambers, J. E., Uhlemann, S. S., & Sorensen, J. P. R. (2015). Optimized arrays for 2-D resistivity survey lines with a large number of electrodes. *Journal of Applied Geophysics*, 112, 136-146.

Marshall, D. J. and Madden, T. R. (1959). Induced polarisation, a study of its causes. *Geophysics*

McGillivray, P., and Oldenburg, D., 1990, Methods for calculating Frechet derivatives and sensitivities for the non-linear inverse problem: A comparative study: *Geophysical Prospecting*, 38, 499-524.

Mufti, I. R., 1976, Finite difference resistivity modeling for arbitrary shaped two dimensional structure, *Geophysics*, vol.41, no. 1, 62-78.

Mufti, I. R., 1978, A practical approach to finite difference resistivity modeling, *Geophysics*, vol.43, no.5, 930-942.

Ngecu, W. M., & Gaciri, S. J. (1995). Lithostratigraphy, provenance and facies distribution of Archaean cratonic successions in western Kenya. *Journal of African Earth Sciences*, 21(3), 359-372.

Ogola, J. S. (1987). Mineralization in the Migori greenstone belt, Macalder, western Kenya. *Geological Journal*, 22(S2), 25-44.

Oldenburg, D. W., & Li, Y. (2005). Inversion for applied geophysics: A tutorial. *Near-surface geophysics: SEG*, 89-150.

Opiyo-Akech, N. (1988). *Geology and geochemistry of the late Archean greenstone belt association, Maseno area, Kenya* (Doctoral dissertation, Ph. D. dissertation 188p. University of Leicester. UK).

Opiyo-Akech, N. (1991). *Geochemical Evidences For The Tectono-magmatic Emplacement Of The Kenyan Greenstone Belt Rocks From The Maseno Area, Western Kenya*.

Parasnis, D. S. (1966). *Mining Geophysics*. Elsevier Publishing Company, Amsterdam.

Reynolds, J. M. (1997). *An introduction to Applied and Environmental Geophysics*. John Wiley and Sons.

Schlumberger, C. (1920). *Etude sur la prospection electrique du sous-sol*. Gauthier-Villars.

- Schlüter, T., & Hampton, C. (1997). *Geology of East Africa* (Vol. 27). Borntraeger.
- Shackleton R. M., 1946. Geology of the Migori gold belt and adjoining areas, Report No. 10, Mining and Geological Department Kenya, Government Printer, Nairobi.
- Siegel, H. O. (1959). Mathematical formulation of type curves for induced polarization.
- Slater, L. D., & Lesmes, D. (2002). IP interpretation in environmental investigations. *Geophysics*, 67(1), 77-88.
- Sternberg, B. K. and Oehler, D. Z. (1990). Induced polarisation in hydrocarbon surveys: Arkoma basin case histories. In Ward, S. H., editor, induced polarization: Applications and Case histories, volume 4. Society of Exploration Geophysicists.
- Stockley, G. M. (1943). The pre-Karoo stratigraphy of Tanganyika. *Geological Magazine*, 80(05), 161-170.
- Sumner, J. S. (1976). Principles of Induced Polarisation for Geophysical Exploration. Elsevier Scientific Publishing Company, Amsterdam.
- Telford, W. M., Geldart, L. P., & Sheriff, R. E. (1976). *Applied geophysics* (Vol. 1). Cambridge university press.
- Towel, J. N., Anderson, R. G., Pelton, W. H., Olhoeft, G. R., and LaBrecque, D. (1985). Direct detection of hydrocarbon contaminants using induced polarization method. SEG meeting, pages 145–147.
- Tsourlos P., 1995, Modelling interpretation and inversion of multielectrode resistivity survey data: Ph.D. Thesis, University of York.
- Uganda Geological Survey, & Harris, N. (1961). *The mineral resources of Uganda*. J. W. Barnes (Ed.).
- Vacquier, V., Holmes, C. R., Kintzinger, P. R., & Lavergne, M. (1957). Prospecting for ground water by induced electrical polarisation. *Geophysics*, 22(3), 660-687.
- Vanhala, H. and Peltoniemi, M. (1992). Spectral ip studies of Finnish ore prospects.
- Wait, J. R. (1959c). The variable–frequency method. In Overvoltage research and geophysical application, volume 4, pages 29–49. Pergomon press, Oxford, England.
- Zhdanov, M. S., & Keller, G. V. (1994). *The geoelectrical methods in geophysical exploration* (Vol. 31). Elsevier Science Limited.